A *Francisella tularensis* L,D-carboxypeptidase plays important roles in cell morphology, envelope integrity, and virulence.

Briana Zellner[1], Dominique Mengin-Lecreulx[2], Brenden Tully[1], William T. Gunning 3rd[3], Robert Booth[3], Jason F. Huntley[1*]

[1] Department of Medical Microbiology and Immunology, University of Toledo, Toledo, OH, U.S.A.; [2] Institute for Integrative Biology of the Cell (I2BC), CEA, CNRS, Univ. Paris-Sud, Université Paris-Saclay, 91198 Gif-sur-Yvette, France; [3]Department of Pathology, University of Toledo, Toledo, OH, U.S.A.

Running Head: *F. tularensis* L,D-carboxypeptidase

To whom correspondence should be addressed: Jason F. Huntley, Department of Medical Microbiology and Immunology, University of Toledo College of Medicine and Life Sciences, 3000 Arlington Ave., MS1021, HEB 200D, Toledo, OH, U.S.A., 43614. Tel.: 419-383-5456; Email: Jason.Huntley@UToledo.edu

Summary

Francisella tularensis is a Gram-negative, intracellular bacterium that causes the zoonotic disease tularemia. Intracellular pathogens, including *F. tularensis*, have evolved mechanisms to survive in the harsh environment of macrophages and neutrophils, where they are exposed to cell membrane-damaging molecules. The bacterial cell wall, primarily composed of peptidoglycan (PG), maintains cell morphology, structure, and membrane integrity. Intracellular Gram-negative bacteria protect themselves from macrophage and neutrophil killing by recycling and repairing damaged PG – a process that involves over 50 different PG synthesis and recycling enzymes. Here, we identified a PG recycling enzyme, L,D-carboxypeptidase A (LdcA), of *F. tularensis* that is responsible for converting PG tetrapeptide stems to tripeptide stems. Unlike *E. coli* LdcA and most other orthologs, *F. tularensis* LdcA does not localize to the cytoplasm and also exhibits L,D-endopeptidase activity, converting PG pentapeptide stems to tripeptide stems. Loss of *F. tularensis* LdcA led to altered cell morphology and membrane integrity, as well as attenuation in a mouse pulmonary infection model and in primary and immortalized macrophages. Finally, an *F. tularensis ldcA* mutant protected mice against virulent Type A *F. tularensis* SchuS4 pulmonary challenge.

Keywords: tularemia, peptidoglycan, L,D-carboxypeptidase, virulence, *Francisella tularensis*

Introduction

The Gram-negative bacterial cell wall plays an important role in maintaining cell shape, protecting against external insults, and preventing cell lysis amid fluctuations in internal turgor pressure (Dhar, 2018). The cell wall is composed of peptidoglycan (PG), a network of alternating *N*-acetylglucosamine (GlcNAc) and *N*-acetylmuramic acid (MurNAc) glycan chains that are crosslinked through peptide stems, and lies just outside of the cytoplasmic membrane of most bacteria (Johnson, 2013; Mengin-Lecreulx & Lemaitre, 2005). In *Escherichia coli*, PG has been shown to be covalently attached to the outer membrane (OM) by Braun's lipoprotein and noncovalently attached by Pal and other lipoproteins (Bouveret, 1999; Braun, 1975; Braun, 1969; Leduc, 1992). A loss of membrane integrity can occur if interactions between PG and attached lipoproteins are disturbed, thus maintenance of correct PG architecture is extremely important (Braun & Hantke, 2019; Braun & Rehn, 1969).

Synthesis of Gram-negative PG precursors, studied mainly in *E. coli*, occurs in the bacterial cytoplasm and requires a series of enzymes to build a pentapeptide PG monomer before transporting this molecule into the periplasm. Periplasmic PG cross-linking most often occurs between the fourth residue (D-Ala) of newly-formed pentapeptide stems to the third residue (*meso*-A_2pm) of existing tripeptide stems (4-3 cross links), resulting in the release of the pentapeptide terminal D-Ala and forming tetrapeptide stems (Glauner, 1988; Pazos & Peters, 2019). PG is not a static structure, rather, PG degradation/remodeling is necessary to incorporate new PG and expand the cell wall during bacterial growth and replication, to insert flagella or secretion systems, and to septate during bacterial division (Scheurwater, 2008). Up to 60% of PG is recycled per generation, helping to repair damaged PG and providing energy during periods of stress or starvation (Dhar, 2018; Holtje, 1998; Park, 2008). Using *E. coli* as a model, more than 50 different PG synthesis and hydrolysis/recycling enzymes have been identified, most of which appear to be

cytoplasmic. While deletion studies in *E. coli* have indicated that some PG synthesis enzymes are essential, few PG hydrolases have been found to be essential and, in fact, substantial redundancy in hydrolase activity appears to exist. Indeed, alterations in cell morphology, membrane integrity, and ability to replicate/divide sometimes are observed only after multiple PG metabolism genes have been deleted (Dhar, 2018; van Heijenoort, 2011; Vollmer & Bertsche, 2008). Given the increasing threat of antimicrobial-resistant organisms and link between PG homeostasis and bacterial virulence, more studies are needed to understand how a diverse range of Gram-negative bacteria synthesize and recycle PG (Juan, 2018). As proof that PG studies can reveal new information about bacterial pathogenesis and new treatment options, an *Acinetobacter baumannii* penicillin-binding protein (PBP) mutant was reported to be more sensitive to complement-mediated killing than wild-type bacteria (Russo, 2009) and a *Helicobacter pylori* PG hydrolase (AmiA) mutant was unable to colonize mouse stomachs (Chaput, 2016).

PG recycling, mainly characterized in *E. coli,* begins with periplasmic lytic transglycosylase (LT) cleavage of the β-1,4-glycosidic linkage between MurNAc and GlcNAc, forming a GlcNAc-1,6-anhydro-MurNAc product, which allows for insertion of new muropeptides and recycling of the GlcNAc-1,6-anhydro-MurNAc peptide (Scheurwater, 2008). Low molecular mass penicillin binding proteins (LMM PBPs) can function as endopeptidases, cleaving the cross-links between adjacent tetrapeptide stems, and/or as D,D-carboxypeptidases, removing the terminal D-Ala of pentapeptides during transpeptidation (cross-linking) reactions, forming the tetrapeptide (Dhar, 2018). Inner membrane permeases, such as AmpG, then transfer GlcNAc-1,6-anhydro-MurNAc disaccharides, with or without attached peptides, to the cytoplasm where they can be disassembled. Cytoplasmic NagZ and AmpD further degrade disaccharides by cleaving the bond between GlcNAc and 1,6-anhydro-MurNAc, and separating the peptide chain from 1,6-anhydro-MurNAc, respectively. Additional cytoplasmic hydrolases, such as L,D-

carboxypeptidases (Ldc), act on free peptide chains to cleave the terminal D-Ala from tetrapeptides, resulting in tripeptides (Dhar, 2018). PG is unusual in that it is both highly dynamic (*e.g.,* allowing for bacterial division and molecular transport across the periplasm), yet tightly regulated to prevent membrane collapse and bacterial death. As such, PG recycling enzymes have been speculated to be important virulence determinants in Gram-negative bacteria (Juan, 2018). Indeed, *E.coli ldc* mutants lyse in stationary phase (Templin, 1999) and are more susceptible to β-lactam antibiotics (Ursinus, 1992), *Helicobacter* and *Campylobacter ldc* mutants have altered cell morphology and defects in motility and biofilm formation (Frirdich, 2012; 2014; Sycuro, 2013), and *Neisseria gonorrhoeae ldc* mutants are unable to stimulate NOD1-dependent responses in the host (Lenz, 2017). However, very little is known about the importance of PG recycling enzymes in the pathogenesis of intracellular pathogens such as *Francisella tularensis*.

F. tularensis, the causative agent of tularemia, is a Gram-negative, intracellular, coccobacillus that can infect and cause lethal disease in many species, including humans (Dennis, 2001; Keim, 2007). There are three subspecies of *F. tularensis*, subsp. *tularensis* (Type A), subsp. *holarctica* (Type B), and subsp. *mediasiatica*, although only subsp. *tularensis* and subsp. *holarctica* are virulent for humans (Kingry, 2014). *F. tularensis* poses a severe threat to public health and has been classified as an NIH Category A Priority Pathogen and a CDC Tier 1 Select Agent due to its low infectious dose (<10 CFU), ease of aerosolization, and high morbidity and mortality rates (up to 60%) (Ellis, 2002; Sjostedt, 2007). Like other intracellular pathogens, *F. tularensis* has evolved different mechanisms to infect, survive, and replicate within host cells, including macrophages and neutrophils (Ray, 2009). However, this lifestyle exposes the bacteria to reactive oxygen species (ROS), reactive nitrogen species (RNS), antimicrobial peptides, and other cell membrane- and cell wall-damaging molecules (Jones, 2012). Our group previously demonstrated that the *F. tularensis* disulfide bond formation protein A (DsbA) ortholog repairs

damaged outer membrane proteins and known virulence factors. We additionally showed that *F. tularensis* DsbA, unlike periplasmic DsbA in *E. coli* and most other Gram-negative bacteria, is outer membrane-bound and is a multifunctional protein with both oxidoreductase and isomerase activities. Finally, using a molecular trapping approach, we identified over 50 *F. tularensis* DsbA substrates, many of which we speculate are involved in virulence (Ren, 2014).

Here, we determined the function of one of those *F. tularensis* DsbA substrates – a previously unstudied hypothetical protein containing a putative LdcA domain – and assessed its role in bacterial virulence. Deletion of *F. tularensis* LdcA resulted in bacteria with altered cell morphology, increased sensitivity to β-lactam antibiotics, yet increased resistance to several stressors (*e.g.,* H_2O_2, NaCl, low pH). Next, we demonstrated that *F. tularensis* LdcA exhibits L,D-carboxypeptidase and L,D-endopeptidase activities on pentapeptide and tetrapeptide residues of PG. Finally, we established that *F. tularensis* LdcA is required for virulence, as mutants were unable to replicate in macrophages or cause disease in mice.

Results

FTL1678 contains a putative L,D-carboxypeptidase domain

Previous studies by our group and others have shown that *F. tularensis* DsbA mutants are attenuated in mice (Qin, 2009; Ren, 2014). However, additional work by our group, demonstrating that DsbA possesses both oxidoreductase and isomerase activities to repair damaged envelope and cell membrane proteins, indicated that other envelope proteins likely are responsible for *F. tularensis* virulence (Ren, 2014). To identify new *F. tularensis* virulence factors, we used a molecular trapping approach and identified over 50 *F. tularensis* DsbA substrates (Ren, 2014). One of those DsbA substrates, FTL1678, is annotated in the *F. tularensis* genome as a conserved membrane hypothetical protein. Here, a conserved domain search revealed that a large portion of

143 FTL1678 contains a putative Ldc domain, part of the peptidase_S66 superfamily (Figure S1). Ldc
144 proteins have been studied in a number of Gram-negative bacteria, including *E. coli* (Metz, 1986a;
145 b; Templin, 1999; Ursinus, 1992), *Pseudomonas aeruginosa* (Korza, 2005), *N. gonorrhoeae* (Lenz,
146 2017), and *Campylobacter jejuni* (Frirdich, 2014). To further explore this conserved domain,
147 amino acid sequences of FTL1678 (*F. tularensis* subsp. *holarctica* [Type B] LVS) and FTT0101
148 (homolog of FTL1678 in *F. tularensis* subsp. *tularensis* [Type A] SchuS4) were aligned with LdcA
149 orthologs from *E. coli*, *P. aeruginosa*, *N. gonorrhoeae*, and *C. jejuni* (named Pgp2). Despite low
150 percentages of amino acid identities among the LdcA orthologs (6.3% to 30.3%; Figure 1), there
151 was a higher degree of amino acid similarity among LdcA orthologs (13.0% [*E. coli* and *C. jejuni*]
152 to 44.7% [*E. coli* and *N. gonorrhoeae*]; Figure 1). Notably, the LdcA Ser-Glu-His catalytic triad,
153 previously shown to be required for *P. aeruginosa* LdcA activity (Korza, 2005), was absent from
154 *C. jejuni* Pgp2 but was present in all LdcA homologs, including FTL1678 and FTT0101 (Figure
155 1).

156 *E. coli* and *P. aeruginosa* Ldcs have been localized to the bacterial cytoplasm (Korza, 2005;
157 Templin, 1999). However, *C. jejuni* Pgp2 is unusual in that it contains a signal peptide and has
158 been speculated to be periplasmic (Frirdich, 2014). In addition, *N. gonorrhoeae* LdcA was found
159 to be periplasmic and outer membrane-associated (Lenz, 2017). As noted above, we previously
160 demonstrated that FTL1678 is a DsbA substrate (Ren, 2014), indicating that FTL1678 is located
161 in the *F. tularensis* envelope (*i.e.,* in the inner membrane [IM], periplasm, or outer membrane
162 [OM]). Bioinformatic analyses of FTL1678 indicated that it is a periplasmic protein due to the
163 presence of a signal peptide but absence of OM or lipoprotein signatures (Table S1). To
164 experimentally confirm FTL1678 localization, we generated an *F. tularensis* strain with 6×
165 histidine-tagged FTL1678, then performed spheroplasting, osmotic lysis, and sucrose density
166 gradient centrifugation to separate IM and OM fractions and probe for protein subcellular

localization. Immunoblotting of whole-cell lysates (WCL), OM fractions, and IM fractions demonstrated that the OM control protein, FopA (Huntley, 2007), only was present in WCL and OM fractions (but not IM fractions; Figure 2) and the IM control protein, SecY (Huntley, 2007), only was present in WCL and IM fractions (but not OM fractions; Figure 2). By comparison, FTL1678 only was detected in WCL and OM fractions, demonstrating OM-association (Figure 2). As noted above, because *N. nonorrhoeae* LdcA was found to fractionate to both the OM and soluble fractions (indicating periplasmic localization) (Lenz, 2017), we next examined the localization of *F. tularensis* periplasmic proteins in our fractions to better understand FTL1678 localization. TolB is a well-known periplasmic protein in Gram-negative bacteria and binds to PG with the peptidoglycan associated lipoprotein, Pal (Clavel, 1998; Walburger, 2002). We previously demonstrated that the *F. tularensis* Pal homolog is OM-localized (Huntley, 2007), similar to its OM-localization in other Gram-negative bacteria. Here, the *F. tularensis* TolB homolog was detected in OM fractions, but not IM fractions (Figure S2), demonstrating that some *F. tularensis* periplasmic proteins fractionate with OMs. Additional fractionation and periplasmic protein localization (Jones et al, 2016) experiments were performed but specific localization of FTL1678 to the periplasm could not be confirmed (data not shown). Regardless, data that FTL1678 is a DsbA substrate (*i.e.,* FTL1678 is an envelope protein)(Ren, 2014), FTL1678 contains a signal peptidase I cleavage site (Table S1), FTL1678 does not contain membrane protein signatures (Table S1), and FTL1678 is OM-associated (Figure 2), provides strong evidence that FTL1678 is not a cytoplasmic protein, unlike *E. coli* LdcA. Instead, our data indicate that, similar to *N. nonorrhoeae* LdcA, FTL1678 may be a periplasmic protein.

FTL1678 exhibits L,D-carboxypeptidase and L,D-endopeptidase activities

To confirm the predicted Ldc activity of FTL1678 and FTT0101, recombinant FTL1678 and FTT0101 were expressed and affinity purified from *E. coli*. As a control, lysates from *E. coli* containing the empty vector (pPROEX HTb) also were affinity-purified . Recombinant FTL1678, lysate from the vector control, or buffer alone were incubated with various PG precursors and PG intermediates (Table 1) to determine substrate specificity and specific activity. The vector control and buffer alone did not demonstrate activity against any of the PG substrates (data not shown). When FTL1678 was incubated with various PG substrates, the highest specific activity was detected against the tetrapeptide substrates GlcNAc-anhydroMurNAc-L-Ala-γ-D-Glu-*meso*-A_2pm-D-Ala (tracheal cytotoxin; TCT; 21.5 nmol/min/mg of protein) and GlcNAc-MurNAc-L-Ala-γ-D-Glu-*meso*-A_2pm-D-Ala (reducing PG monomer; 15.6 nmol/min/mg of protein), confirming that FTL1678 exhibits L,D-carboxypeptidase activity (Table 1). Interestingly, FTL1678 activity against free tetrapeptide, L-Ala-γ-D-Glu-*meso*-A_2pm-D-Ala, was approx. 6-fold lower (3.4 nmol/min/mg of protein) than TCT and 5-fold lower than the reducing PG monomer (Table 1), indicating that GlcNAc and MurNAc may be important for tetrapeptide recognition or FTL1678 binding. Importantly, FTL1678 exhibited specific activity against pentapeptide substrates MurNAc-L-Ala-γ-D-Glu-*meso*-A_2pm-D-Ala-D-Ala (9.8 nmol/min/mg of protein; Table 1) and UDP-MurNAc-L-Ala-γ-D-Glu-*meso*-A_2pm-D-Ala-D-Ala (5.9 nmol/min/mg of protein; Table 1), indicating that FTL1678 also functions as an L,D-endopeptidase (cleavage of the pentapeptide between *meso*-A_2pm and D-Ala) by FTL1678.

To further investigate the endopeptidase activity of FTL1678, FTL1678 was incubated with various TCT monomer and dimer substrates, containing different peptide lengths and cross-link locations (Table S2). Although FTL1678 exhibited the highest specific activity against TCT monomers containing tetrapeptide stems with either an Alanine or a Glycine in the fourth position

(20 nmol/min/mg and 18 nmol/min/mg of protein, respectively), FTL1678 also was able to cleave all four variations of the TCT dimer (two cross-linked TCT monomers), demonstrating endopeptidase activity (Table S2). Of the four different TCT dimers tested, FTL1678 was most active on TCT dimers connected by a 4-3 cross linkage (6.6 nmol/min/mg of protein), followed by an approx. 24-fold reduction in activity on 3-3 cross links connecting two tripeptides (0.28 nmol/min/mg of protein), a tripeptide and tetrapeptide with a Glycine at the fourth position (0.21 nmol/min/mg of protein), and a tripeptide and tetrapeptide with an Alanine at the fourth position (0.16 nmol/min/mg of protein) (Table S2). These data suggest that, while FTL1678 exhibits endopeptidase activity on 4-3 and 3-3 cross-links, cleavage of 3-3 cross links is likely not its main physiological function.

Finally, FTL1678 had negligible activity against L-lysine-containing substrates (0.7 to 1.3 nmol/min/mg of protein; Table 1), where L-lysine replaced *meso*-A_2pm at the third amino acid position, indicating the importance of *meso*-A_2pm. Assays were repeated with recombinant FTT0101 (SchuS4 homolog) and, due to 99.4% amino acid identify with FTL1678, FTT0101 demonstrated similar tetrapeptide cleavage activity (*i.e.,* LdcA activity) as FTL1678 (Table 1). FTT0101 also was not active on a peptidoglycan polymer and had either no or negligible activity on PG monomers that were amidated at the *meso*-A_2pm or D-Glu residues (Table 1). Additionally, FTT0101 was not inhibited by 5 mM EDTA and did not require the presence of cations (Mg^{2+}) for tetrapeptide cleavage (data not shown).

FTL1678 controls bacterial morphology

LdcA has been shown to be important for maintenance of bacterial morphology and structural integrity (Frirdich, 2014; Sycuro, 2013). In addition, mutations/deletions or combinations of mutations/deletions in PG-modifying proteins can result in abnormal bacterial

morphology, emphasizing the importance of PG modification and recycling (Guinane, 2006; Heidrich, 2001; Juan, 2018; Nelson, 2000; Priyadarshini, 2007; Sycuro, 2010). To assess if FTL1678 plays a similar role in *F. tularensis*, we generated an isogenic deletion of *FTL1678*, referred to hereafter as Δ*FTL1678*, in *F. tularensis* LVS. When examined by transmission electron microscopy (TEM), wild-type (WT) bacterial width ranged from 350 to 800 nm (Figures 3A and 3D), whereas Δ*FTL1678* bacteria were more uniform in cell width, averaging approx. 350 nm (Figures 3B and 3D). WT bacteria were observed to be coccobacilli with loosely-associated OM (Figure 3A), while Δ*FTL1678* bacteria were found to be more coccoid in appearance, the OM was tightly-associated, and three prominent structures were present around the periphery of each bacterium, likely the OM, PG, and IM (Figure 3B). Additionally, Δ*FTL1678* bacteria appeared more electron dense and had a significantly-thicker OM than WT bacteria (Figures 3A, 3B, and 3C).

Previous studies have shown that deletion of genes for PG-modifying proteins (*e.g.,* murein hydrolases) can result in abnormal growth characteristics, including lysis during stationary phase (Templin, 1999) and an inability to separate daughter cells at the septa during cell division, resulting in abnormal bacterial chains (Chaput, 2016; Denome, 1999; Heidrich, 2001; 2002; Juan, 2018; Priyadarshini, 2007; 2006). Although *N*-acetylmuramyl-L-alanine amidases have been shown to be predominantly involved in the cleavage of bacterial septa, deletion of lytic transglycosylases and some endopeptidases, in combination with amidase deletions, also have resulted in abnormal bacterial chains (Heidrich, 2001; 2002). To examine any potential replication defects of Δ*FTL1678*, we compared both OD_{600} values (Figure S3A) and CFUs over time (Figure S3B) of WT and Δ*FTL1678* in supplemented Mueller Hinton Broth (sMHB; standard growth medium for *F. tularensis*; (Huntley, 2007)), finding that Δ*FTL1678* did not have any inherent growth defects. When examining both WT and Δ*FTL1678* by TEM for any septation defects or

abnormal bacterial chains, approximately 10% of Δ*FTL1678* bacteria grew in chains of three to four bacteria (Figure S4A and S4B), whereas no WT bacteria exhibited this septation defect (data not shown). Taken together, our findings that Δ*FTL1678* is 1.5- to 2-times smaller than WT (Figure 3D), Δ*FTL1678* is more coccoid in shape (Fig 3B), Δ*FTL1678* has a pronounced three-layered envelope, including a prominent electron dense layer between the IM and OM (likely PG; Figure 3B), and Δ*FTL1678* has a partial septum defect (Figure S4), further support the role of FTL1678 as a PG-modifying enzyme that is important for bacterial elongation and division.

Deletion of FTL1678 affects antibiotic, detergent, and stressor sensitivity

Given the above noted morphological differences in the Δ*FTL1678* envelope (*e.g.,* thicker OM; tightly-associated OM; three prominent envelope structures) using TEM, we assessed envelope (*i.e.,* IM, PG, and OM) integrity by growing both WT and Δ*FTL1678* bacteria in the presence of various antibiotics, detergents, and dyes, and measuring zones of inhibition after 48 h of growth (Table 2). Δ*FTL1678* was found to be more susceptible than WT to ampicillin, vancomycin, lysozyme, and SDS (Table 2), indicating potential changes to PG (ampicillin sensitivity), OM integrity (vancomycin and lysozyme sensitivity), or efflux pumps (SDS sensitivity). Conversely, Δ*FTL1678* was found to be more resistant than WT to gentamicin, tetracycline, chloramphenicol, ciprofloxacin, ethidium bromide, and Triton X-100 (Table 2). Given that the majority of these latter reagents must enter the cytoplasm to exert their inhibitory effects (*i.e.,* gentamicin, tetracycline, and chloramphenicol inhibit protein synthesis; ciprofloxacin and ethidium bromide interfere with DNA replication), these results suggest that Δ*FTL1678* bacteria exclude these inhibitory molecules from entering the cytoplasm.

To better understand potential differences in the Δ*FTL1678* envelope, WT and Δ*FTL1678* were grown in either sMHB at 37°C or in sMHB with various stress conditions. In sMHB at 37°C,

Δ*FTL1678* did not exhibit a growth defect but, instead, appeared to grow to a higher optical density (OD_{600}) than WT (Figure 4A). However, as noted above, despite higher OD_{600} measurements for Δ*FTL1678* at several time points, bacterial numbers were not significantly different between WT and Δ*FTL1678* (Figure S3). Although speculative, the disassociation between Δ*FTL1678* optical densities and bacterial numbers may be due to the observed TEM morphological differences of Δ*FTL1678* (Figure 3 and Figure S4). Compared with growth in sMHB at 37°C, no substantial differences in the growth rates of WT and Δ*FTL1678* were observed at either 40°C or in the presence of 60 μM $CuCl_2$ (Figure 4B and 4C). However, Δ*FTL1678* grew considerably better than WT in the presence of 5 mM H_2O_2, 5% NaCl, and pH 5.5 (Figure 4D, 4E, and 4F, respectively), providing further evidence of modifications to the Δ*FTL1678* envelope. Although many mechanisms can account for increased resistance to H_2O_2, high NaCl, and low pH, the combined results from these antibiotic, detergent, and stressor sensitivity/resistance assays suggest that Δ*FTL1678* bacteria may have decreased OM integrity, altered PG, altered activity of efflux pumps, and a less permeable IM. Indeed, decreased permeability of the IM and altered activity of IM efflux pumps may help explain the more electron-dense staining of Δ*FTL1678*, compared to WT (Figure 3).

*Δ*FTL1678 is fully-attenuated in a mouse pulmonary infection model*

To examine if FTL1678 plays a role in *F. tularensis* virulence, mice were intranasally infected with 10^4 CFU of either WT or Δ*FTL1678* and monitored daily for signs of disease. Whereas all WT-infected mice died by day 9 post-infection (median time-to-death day 6), Δ*FTL1678* was completely attenuated (100% survival through day 21 post-infection), demonstrating that FTL1678 is required for *F. tularensis* virulence (Figure 5A). To confirm that the observed attenuation was solely due to the deletion of *FTL1678*, and not to polar effects, we

complemented Δ*FTL1678* with a 6× His-tagged FTL1678 *in trans*, which fully-restored virulence to WT levels (all mice died by day 7; median time-to-death day 6; Figure 5A).

To more carefully assess Δ*FTL1678* attenuation *in vivo*, we intranasally-infected mice with 10^4 CFU of either WT LVS or Δ*FTL1678*, and enumerated bacterial CFUs from lungs, livers, spleens, and blood on days 2 and 5 post-infection to examine bacterial replication and dissemination to these organs/tissues over time. On day 2 post-infection, WT LVS replicated to $>10^7$ CFU/mg lung and had disseminated to livers, spleens (approx. 10^3 CFU/mg), and blood (10^3 CFU/ml; Figure 5B). In contrast, Δ*FTL1678* had an initial (day 2) colonization defect in the lungs (4-logs less than WT) and was unable to disseminate to livers, spleens, or blood (Figure 5B). By day 5 post-infection, the attenuation of Δ*FTL1678* was even more apparent, with WT LVS replicating to extremely high numbers (approx. 10^8 CFU/mg) in lungs, livers, and spleens, compared with Δ*FTL1678,* which replicated approx. 1-log in lungs (between day 2 and 5), but was 4-log attenuated in lungs and was not detectable in livers or spleens (Figure 5B). Although Δ*FTL1678* was detected in the blood on day 5, it was 2-logs less than WT LVS (Figure 5B).

The Type A *F. tularensis* strain SchuS4 originally was isolated from a human tularemia patient and requires BSL3 containment. Given its relevance to human disease, we next generated an isogenic deletion mutant of the *FTL1678* homolog, *FTT0101*, in SchuS4. When mice were intranasally-infected with either WT SchuS4 or Δ*FTT0101,* all mice died by day 7 post-infection, indicating that *FTT0101* is not required for SchuS4 virulence (Figure S5). Whereas Δ*FTT0101*-infected mice exhibited a slightly delayed time-to-death (median time-to-death day 6; Figure S5), compared with WT SchuS4-infected mice (median time-to-death day 5; Figure S5), this may be due to differences in the infectious dose administered to mice in this experiment (80 CFU SchuS4; 12 CFU Δ*FTT0101*). However, it also remains possible that the extreme virulence of SchuS4 (intranasal LD_{50} <10 CFU in our hands) complicates assessments of mutant attenuation *in vivo*.

To further assess Δ*FTT0101*, the susceptibilities of Δ*FTT0101* and WT SchuS4 to various antibiotics, detergents, and dyes were compared, with no significant differences observed (Table S3). At this time, we cannot fully explain why the *F. tularensis* Type B LdcA mutant Δ*FTL1678* is fully-attenuated in mice (Figure 5) and displays altered sensitivity/resistance to antibiotics, detergents, and dyes (Table 2), while the *F. tularensis* Type A LdcA mutant Δ*FTT0101* retains virulence in mice (Figure S5) and does not demonstrate altered sensitivity/resistance to antibiotics, detergents, and dyes (compared to WT SchuS4; Table S3). However, this finding is not unexpected given genomic studies indicating that, despite >97% nucleotide identity between Type A and Type B *F. tularensis*, there are over 100 genomic rearrangements between Type A and Type B and each subspecies encodes over 100 unique genes that likely influence known differences in Type A and Type B virulence (Petrosino et al, 2006).

Putative FTL1678 catalytic triad and Ldc activity are required for F. tularensis virulence

As noted above and highlighted in Figure 1, *P. aeruginosa* LdcA contains a Ser-Glu-His catalytic triad which is essential for function and is characteristic of Ldc in the Peptidase_S66 family (Korza, 2005). The Ser-Glu-His catalytic triad also has been confirmed in Ldc from *E. coli* (Meyer, 2018), *Novosphingobium aromaticivorans* (Das, 2013), and *N. gonorrhoeae* (Lenz, 2017). Given the relatively conserved spacing of Ser134-Glu239-His308 residues in FTL1678 (Figure 1), we tested if these residues were required for *F. tularensis* virulence (similar to Figure 5A virulence assessments for Δ*FTL1678* and the FTL1678 complemented strain). Site-directed mutagenesis was performed to independently generate FTL1678 complementation constructs containing either S134A, E239A, or H308A mutations. Next, Δ*FTL1678* was complemented *in-trans* with each of these FTL1678 catalytic triad point mutants, and mice were intranasally infected with either WT, Δ*FTL1678*, Δ*FTL1678 trans*-complemented with *FTL1678*, or Δ*FTL1678 trans*-complemented

with one of the FTL1678 catalytic triad point mutants (referred to hereafter as S134A, E239A, and H308A). Confirming our previous findings, Δ*FTL1678* was completely attenuated (100% survival through day 21), while complementation of Δ*FTL1678* with either FTL1678 (all mice dead by day 8), S134A (all mice dead by day 7), E239A (all mice dead by day 8), or H308A (all mice dead by day 8), fully-restored virulence to WT LVS levels (all mice dead by day 10; Figure S6). These results indicated that although a putative Ser-Glu-His catalytic triad is present in FTL1678, mutation of individual residues does not affect *F. tularensis* virulence *in vivo*.

Given the complexity of *in vivo* animal infections and the possibility that single mutations in the putative Ser134-Glu239-His308 catalytic triad may not be sufficient to abolish enzyme function or alter bacterial virulence, we next assessed if mutations of two or three residues in the putative catalytic triad affected *in vitro* enzyme activity. Recombinant FTL1678 mutant proteins were generated and purified, each containing either two amino acid mutations (S134A/E239A, S134A/H308A, and E239A/H308A) or three amino acid mutations (S134A/E239A/H308A). Similar to what is described above, enzymatic assays were performed, using the TCT monomer as a substrate. While no specific activity to TCT monomer was detected for the empty vector control or buffer alone, WT FTL1678 was active against the TCT monomer (11.0 nmols/min/mg). By comparison, no activity was detected for any of the double or triple mutant proteins (Table S4), suggesting that two or more of the catalytic triad residues are required for FTL1678 Ldc activity.

The Ldc ortholog alignment (Figure 1) highlighted that, of the six Ldc orthologs examined here, only *C. jejuni* Pgp2 lacked the Ser-Glu-His catalytic triad. However, *C. jejuni* Pgp2 has been shown to exhibit LdcA activity (Frirdich, 2014), indicating that a Ser-Glu-His catalytic triad is not required for LdcA function. To test if an LdcA ortholog, without the Ser-Glu-His catalytic triad, could restore virulence in the Δ*FTL1678* mutant, we complemented Δ*FTL1678* with a 6× His-tagged Pgp2 from *C. jejuni* and infected mice with either WT LVS, Δ*FTL1678*, Δ*FTL1678 trans*-

383 complemented with FTL1678, or Δ*FTL1678 trans*-complemented with *C. jejuni* Pgp2. While
384 Δ*FTL1678* was fully attenuated (100% survival through day 21), the Pgp2 *trans*-complement was
385 fully-virulent (median time-to-death 6 days; all mice dead by day 7), nearly identical to WT LVS
386 (median time-to-death 7 days; all mice dead by day 7) and the FTL1678 *trans*-complement
387 (median time-to-death 6 days; all mice dead by day7; Figure 5C). This *in vivo* data provides further
388 evidence that FTL1678 is an Ldc and Ldc activity is required for *F. tularensis* virulence.

389 To provide additional evidence that FTL1678 exhibits Ldc activity and that *C. jejuni* Pgp2
390 functionally complements Δ*FTL1678*, the FTL1678 *trans*-complement and Pgp2 *trans*-
391 complement were examined by TEM, revealing that both complemented strains had similar
392 morphology as WT LVS (Figure S7A and S7B; Figure 3A). Additionally, OM thickness and cell
393 width were measured for WT, Δ*FTL1678*, and both complemented strains, demonstrating that both
394 complemented strains had OM thicknesses and cell widths similar to WT, and both complemented
395 strains were significantly different from Δ*FTL1678* (Figure S7C and S7D). Finally, when grown
396 in the presence of various stressors (*e.g.,* 5 mM H_2O_2, 5% NaCl, pH 5.5, antibiotics, SDS,
397 lysozyme, or ethidium bromide), both complemented strains exhibited similar phenotypes as WT
398 LVS (Figure S8A-D and Table S5). Taken together, these studies indicated that at least two
399 residues of the putative Ser134-Glu239-His308 catalytic triad are required for FTL1678 LdcA
400 enzymatic activity. These studies also demonstrated that an LdcA ortholog can functionally
401 complement Δ*FTL1678,* further supporting that FTL1678 is an LdcA ortholog.

402

403 *FTL1678 is required for F. tularensis replication in macrophages*

404 *F. tularensis* is an intracellular pathogen and macrophages appear to be one of the major
405 targets for *F. tularensis* infection and replication (De Pascalis, 2018; Hall, 2008; Steiner, 2017).
406 To investigate potential replication defects of Δ*FTL1678* in macrophages, J774A.1 macrophages

or murine bone marrow-derived macrophages (mBMDM) were infected with either WT LVS or Δ*FTL1678* (MOI 100:1) and bacterial numbers were enumerated at 0 h (entry), 6 h, and 24 h post-infection. At entry (0 h), approx. 2.5-logs more Δ*FTL1678* were present in both macrophage lines, compared with WT LVS (Figure 6A). This likely was due to the above noted gentamicin resistance of Δ*FTL1678* (Table 2). Attempts to normalize entry numbers for both WT LVS and Δ*FTL1678*, using different antibiotics or combinations of antibiotics, were not successful. Despite higher numbers of Δ*FTL1678* in both macrophages at entry (0 h) and 6 h, Δ*FTL1678* was unable to replicate in either macrophage, and decreased approx. 1-log from 6 h to 24 h (Figure 6A). By comparison, WT LVS numbers increased 1.5- to 2-logs from 6 h to 24 h (Figure 6A). To normalize WT LVS and Δ*FTL1678* bacterial numbers and replication rates in both macrophages, fold change in bacterial numbers was calculated from 6 h to 24 h: WT was found to increase 2.5- and 1.5-logs in J774A.1 and mBMDMs, respectively, whereas Δ*FTL1678* was found to decrease 0.5- to 1-log, respectively (Figure 6B). Taken together, these *in vitro* results (Figures 6A and 6B) confirm the observed *in vivo* attenuation of Δ*FTL1678* (Figures 5A and 5B).

ΔFTL1678 protects mice against Type A F. tularensis infection

No FDA-approved vaccine currently is available to prevent tularemia. In addition, *F. tularensis* is designated as an NIH Category A priority pathogen and CDC Tier 1 Select Agent, highlighting the extreme virulence of this bacterium and the need for a safe and effective vaccine to prevent tularemia. Given our above findings that 10^5 CFU of Δ*FTL1678* did not cause disease or death in mice (Figures 5A and 5C), we next examined whether high doses (10^7 or 10^9 CFU) of Δ*FTL1678* were attenuated or if Δ*FTL1678* immunization could protect mice from fully-virulent Type A *F. tularensis* SchuS4 challenge. First, all mice intranasally immunized with either 10^5, 10^7, or 10^9 CFU of Δ*FTL1678* survived through day 28 post-infection, with no signs of clinical

disease (Figure 7A). Next, on day 29, all mice were boosted with 10^9 CFU of Δ*FTL1678* and no mice demonstrated any signs of disease through day 50 (Figure 7A). Finally, on day 51, mice were intranasally-challenged with 120 CFU (6× the LD_{50}) of SchuS4 and the health status of each immunization group was monitored for 26 days post-challenge. In a dose-dependent manner, the 10^9 prime-10^9 boost regimen conferred 80% protection, the 10^7 prime-10^9 boost regimen conferred 40% protection, and the 10^5 prime-10^9 boost regimen conferred 20% protection (Figure 7B). These data demonstrate that Δ*FTL1678* is highly attenuated (up to 10^9 CFU) and that Δ*FTL1678* may be able to be used as a live, attenuated vaccine.

ΔFTL1678 does not cause tissue damage

The *in vitro* (Figure 6) and *in vivo* (Figures 5A, 5B, 7A) attenuation of Δ*FTL1678,* as well as protection against SchuS4 pulmonary challenge (Figure 7B), indicated that Δ*FTL1678* could be used as a live, attenuated vaccine. While live, attenuated vaccines have been extremely effective at preventing a number of diseases, they can pose safety challenges (Minor, 2015; Roberts, 2018). To assess whether Δ*FTL1678* immunization induced any pathology in immunized mice, lungs, livers, and spleens from uninfected, WT LVS-, or Δ*FTL1678*-infected mice were assessed for pathologic changes on day 5 post-infection/immunization. Day 5 is when mice exhibit severe signs of disease and is one day before the majority of WT-infected mice begin succumbing to disease (Figures 5 and 7). WT LVS-infected lungs demonstrated alveolar wall thickening, large areas of inflammation, and severe neutrophil infiltration (Figure 8A). By comparison, little inflammation was observed in Δ*FTL1678*-infected lungs, although some red blood cell congestion was present, indicating a limited, acute immune response that was quickly resolved (Figure 8A). Whereas WT LVS-infected livers were characterized by diffuse inflammation with focal areas of necrosis, Δ*FTL1678*-infected livers were virtually indistinguishable from uninfected livers, with

455 no observable pathology (Figure 8A). Finally, although the architecture of WT LVS-infected
456 spleens lacked distinct areas of white pulp or red pulp, indicative of a severe infection, Δ*FTL1678*-
457 infected spleens were observed to contain distinct areas of red pulp and white pulp, with some red
458 blood cell congestion – indicating a limited, acute immune response that was quickly resolved
459 (Figure 8A). All tissues were blindly scored using a pathology severity index (scale from 0 to 4,
460 with 4 indicating severe pathology), confirming that Δ*FTL1678*-infected tissues were virtually
461 indistinguishable from uninfected tissues (pathology scores of 1 for lungs, 0 for liver, and 1.5 for
462 spleens) and WT LVS-infected tissues had significantly higher pathology scores (pathology scores
463 >3.5 for all tissues; Figure 8B).
464
465 **Discussion**
466 Bacterial PG is a complex, mesh-like structure, composed of a glycan backbone,
467 crosslinked to varying degrees, by peptide chains (de Pedro, 2015). It is well known that this
468 structure plays an important role in maintaining Gram-negative bacterial cell morphology,
469 membrane integrity, regulating changes in osmotic pressure, and providing a platform for
470 attachment of the OM (den Blaauwen, 2008; Silhavy et al, 2010). Although a majority of PG
471 studies have focused on how the thick layer of PG in Gram-positive bacteria contributes to
472 virulence and antibiotic resistance, more recent studies have highlighted that Gram-negative PG
473 also is intimately linked with pathogenicity (Juan, 2018).
474 PG recycling is an essential function of Gram-negative bacteria during cell growth and
475 division to produce new cell wall components. In fact, Gram-negative bacteria recycle up to 60%
476 of their PG with every generation, suggesting that both PG synthesis and PG recycling are dynamic
477 (Dhar, 2018; Typas, 2011). A number of proteins are involved in these processes and, while they
478 are well-characterized in *E. coli*, very little is known about these pathways in intracellular

pathogens such as *Burkholderia pseudomallei*, *Legionella pneumophila*, or *F. tularensis* (Jenkins, 2019; Kijek, 2019; Spidlova, 2018; van Heijenoort, 2011).

E. coli LdcA, a cytoplasmic protein, was the first L,D-carboxypeptidase to be identified and was shown to be important for PG recycling and survival during stationary phase (Templin, 1999; Ursinus, 1992). More recently, Ldc orthologs have been identified in *P. aeruginosa* (Korza, 2005), *C. jejuni* (Frirdich, 2014), *N. gonorrhoeae* (Lenz et al, 2017), and *N. aromaticivorans* (Das, 2013). In this study, we identified an *F. tularensis* Ldc ortholog, FTL1678, which we propose naming LdcA based on its confirmed L,D, carboxypeptidase activity (Table 1) and role in maintaining bacterial morphology. Unlike well-characterized cytoplasmic LdcA orthologs from *E. coli* and *P. aeruginosa*, we demonstrated that *F. tularensis* LdcA was localized to OM fractions and, given co-localization with PG-associated proteins Pal and TolB, is most likely located on the inner leaflet of the OM or in the periplasm (associated with PG). At this time, we can only speculate on the OM-association or periplasmic localization of *F. tularensis* LdcA, but in the context of PG repair and recycling, periplasmic LdcA certainly offers a fitness advantage. In addition, this is not the first report of a periplasmic LdcA, as *C. jejuni* Pgp2 is predicted to be periplasmic and *N. gonorrhoeae* LdcA previously was reported to be periplasmic (Frirdich, 2014; Lenz, 2017).

Our results demonstrated, for the first time, that *F. tularensis* LdcA directly acts on the TCT tetrapeptide and the reducing PG monomer. More importantly, we demonstrated that *F. tularensis* LdcA directly cleaves PG pentapeptides to tripeptides, without a prior cleavage event by a D,D-carboxypeptidase/penicillin binding protein (PBP), such as DacD, and that FTL1678 cleaves TCT dimers with 4-3 and 3-3 cross links, highlighting that *F. tularensis* LdcA is a multi-functional enzyme that performs both L,D-carboxypeptidase and L,D- and D,D-endopeptidase activities (Table 1 and Table S2). . It should be noted that although *N. gonorrhoeae* LdcA has

been reported to have L,D-endopeptidase activity, this activity is specific to tetrapeptide cross links (3-3 cross links) (Lenz, 2017). Interestingly, only two previous studies have examined putative *F. tularensis* PG modifying enzymes and both studies primarily focused on the role of an *F. tularensis* DacD ortholog in virulence, with no PG activity assays to confirm function (Kijek, 2019; Spidlova, 2018). In our PG cleavage analysis, *F. tularensis* LdcA demonstrated the highest specific activity on disaccharide-tetrapeptide PG substrates (GlcNAc-anhydroMurNAc-L-Ala-γ-D-Glu-*meso*-A_2pm-D-Ala [TCT] and GlcNAc-MurNAc-L-Ala-γ-D-Glu-*meso*-A_2pm-D-Ala [reducing PG monomer]), followed by cleavage of pentapeptide PG substrates (MurNAc-L-Ala-γ-D-Glu-*meso*-A_2pm-D-Ala-D-Ala and UDP-MurNAc-L-Ala-γ-D-Glu-*meso*-A_2pm-D-Ala-D-Ala). Despite high specific activity of *F. tularensis* LdcA on tetrapeptide attached to the disaccharide, *F. tularensis* LdcA demonstrated approximately 6-times lower specific activity on free tetrapeptide (no sugars) (Table 1). In contrast, *E. coli* LdcA has been shown to have the highest specific activity on free tetrapeptide, monosaccharide-tetrapeptide (MurNAc-L-Ala-γ-D-Glu-*meso*-A_2pm-D-Ala), and monosaccharide tetrapeptide linked to a glycan lipid carrier (UDP-MurNAc-tetrapeptide) (Templin, 1999), but is unable to cleave dimeric muropeptides. Additionally, *F. tularensis* LdcA was active against TCT dimers (two crosslinked TCT monomers), cleaving the 4-3 cross linkage between D-Ala and A_2pm and the 3-3 cross linkage between A_2pm and A_2pm, but was not active on PG polymers. This TCT dimer cleavage indicates that, in addition to L,D carboxypeptidase activity, *F. tularensis* LdcA possesses L,D- and D,D-endopeptidase activity on peptide cross-links.

Previous studies have shown that Ldc orthologs are important for bacterial morphology and membrane integrity. Deletion of the *ldc* orthologs *csd6* from *H. pylori* (Sycuro, 2013) and *pgp2* from *C. jejuni* (Frirdich, 2014) resulted in loss of helical morphology. Here, we demonstrated that FTL1678 is essential for maintaining both the size (width) and the coccobacillus morphology of *F. tularensis,* as Δ*FTL1678* were significantly-smaller than WT and exhibited a more-rounded,

cocci shape than WT (Figure 3). Further evidence for the role of *F. tularensis* LdcA in modifying and recycling PG, which impacts bacterialmorphology, is provided by TEM images of Δ*FTL1678* bacteria that had prominent three-layered structures at their periphery, including a thick middle layer (presumably PG), compared to WT (Figure 3). In Δ*FTL1678* bacteria, it is possible that loss of LdcA activity may have reduced PG recycling or may have affected the breakdown of existing PG (important for cell division), resulting in a buildup of pentapeptides or tetrapeptides that are highly-crosslinked. Our lab and others have repeatedly attempted to isolate and analyze *F. tularensis* PG but theses attempts have not been unsuccessful (data not shown; Martin Pavelka, U. Rochester, personal communication). As such, we can only speculate on the true nature of the thick PG and OM layers in Δ*FTL1678* (Figure 3).

Because Δ*FTL1678* bacteria were found to have a thicker OM (Figure 3C), a prominent middle layer in their envelope (presumably PG; Figure 3B), and altered cell morphology (Figure 3B), we investigated differences in WT and Δ*FTL1678* susceptibility to various antibiotics, detergents, and stressors. Vancomycin and lysozyme, usually not effective against Gram-negatives due to their inability to penetrate the OM, inhibited Δ*FTL1678* growth (Table 2), indicating increased permeability of the Δ*FTL1678* OM. Vancomycin, in particular, may have been effective on Δ*FTL1678* because its mechanism of action includes binding to the two terminal D-Ala-D-Ala residues of PG pentapeptide chains and preventing cross-linking of monomers. Δ*FTL1678* may have increased amounts of pentapeptides present in its PG, providing more targets for vancomycin action. Similarly, ampicillin inhibits bacterial transpeptidases, which blocks cross-linking of peptide side chains of PG strands. Taken together, the enhanced susceptibility of Δ*FTL1678* bacteria to vancomycin and ampicillin supports the role of *F. tularensis* LdcA as a PG-modifying enzyme. Conversely, Δ*FTL1678* was more resistant to antibiotics and molecules that must cross the IM to exert their toxic effects, including gentamicin, tetracycline, chloramphenicol,

551 ciprofloxacin, and ethidium bromide (Table 2), suggesting that Δ*FTL1678* bacteria have a less
552 permeable IM. Mechanisms to explain why Δ*FTL1678* bacteria were more resistant to other
553 stressors, including Triton X-100, H_2O_2, high salt, and low pH, are less clear, but could include
554 increased expression/activity of chaperone proteins, efflux pumps, antioxidant/scavenger proteins,
555 and membrane stabilizing proteins (Knodler et al, 2003; Lund et al, 2014; Mishra & Imlay, 2012).
556 The extreme virulence of Type A *F. tularensis* and its designation as a Tier 1 Select Agent
557 highlight why studies to identify *F. tularensis* virulence factors and the development of new
558 vaccines is important. In this study, we identified the role of a previously unstudied protein,
559 FTL1678, in PG recycling, PG integrity, and bacterial morphology. In addition, we found that
560 FTL1678 was required for *F. tularensis* LVS virulence and demonstrated that Δ*FTL1678*
561 conferred 80% protection against fully-virulent, Type A *F. tularensis* SchuS4 pulmonary
562 challenge. Further studies are needed to determine specific immune responses induced by
563 Δ*FTL1678* immunization, as well as to identify the most effective immunization regimen (*e.g.,*
564 number of immunizations and time between immunizations).
565 Finally, given our findings that PG maintenance and recycling are important for *F.*
566 *tularensis* virulence, and that future studies may reveal additional PG-associated enzymes, we used
567 bioinformatic approaches to predict other proteins involved in *F. tularensis* PG synthesis and
568 recycling (Figure 9). While at least seven PG synthesis and recycling genes/proteins orthologs
569 could not be identified, 22 putative PG synthesis and recycling proteins were identified in *F.*
570 *tularensis* (Figure 9). Of these, only DacD (FTL1060/FTT1029) has been studied in *F. tularensis*.
571 Given our observed attenuation of Δ*FTL1678*, future studies to better understand PG synthesis and
572 recycling pathways may offer more opportunities to better understand the virulence of *F. tularensis*
573 and other intracellular pathogens. Characterization of other proteins involved in PG pathways may

574 provide clues as to why *F. tularensis* LdcA is OM-associated or periplasmic and encodes both
575 L,D-carboxypeptidase and L,D-endopeptidase activities.
576
577
578 **Experimental Procedures**
579 *Bacterial strains and culture conditions*
580 *F. tularensis* Type A strain SchuS4 and *F. tularensis* Type B strain LVS were obtained from BEI
581 Resources and cultured as previously described (Ren, 2014; Wu, 2016). All experiments with
582 SchuS4 were performed under BSL3 containment conditions at the University of Toledo Health
583 Science Campus BSL3 laboratory. Routine *F. tularensis* cultures were grown overnight at 37°C
584 with 5% CO_2 on supplemented Mueller-Hinton agar (sMHA): Mueller-Hinton broth powder
585 (Becton Dickinson) was mixed with 1.6% (wt/vol) Bacto Agar (Becton Dickinson), autoclaved,
586 and further supplemented with 2.5% (vol/vol) bovine calf serum (Hyclone), 2% (vol/vol)
587 IsoVitaleX (Becton Dickinson), 0.1% (wt/vol) glucose, and 0.025% (wt/ vol) iron pyrophosphate.
588 For mouse infections, *F. tularensis* was first grown on sMHA then transferred to Brain Heart
589 Infusion agar (BHI; Becton Dickinson). Chocolate agar for mutant strain generation was prepared
590 by mixing Mueller Hinton broth powder with 1.6% (wt/vol) agar, 1% (wt/vol) tryptone, and 0.5%
591 (wt/vol) sodium chloride, autoclaved, and further supplemented with 1% (wt/vol) hemoglobin and
592 1% (vol/vol) IsoVitaleX. For macrophage infections, *F. tularensis* was first grown on sMHA then
593 transferred to modified chocolate agar: Mueller-Hinton broth powder was mixed with 1.6%
594 (wt/vol) Bacto Agar, 1% hemoglobin (wt/vol), and 1% (vol/vol) IsoVitaleX. All growth curves
595 were performed in sMHB: Mueller-Hinton broth powder was mixed with 182 mg/L calcium
596 chloride dihydrate, and 210 mg L^{-1} magnesium chloride hexahydrate, 0.1% (wt/vol) glucose,
597 0.025% (wt/vol) iron pyrophosphate, and 2% (vol/vol) IsoVitaleX. All bacterial strains and

plasmids are listed in Table S6. *E. coli* S17-1 and *E. coli* NEB10-β were grown in Luria Bertani (LB) broth or on LB agar at 37°C, supplemented as needed with antibiotics.

Sequence Alignments and Bioinformatic Predictions

Amino acid alignments of *F. tularensis* subsp. *holarctica* FTL_1678, *F. tularensis* subsp. *tularensis* FTT_0101, *E. coli* LdcA (BAA36050.1), *P. aeruginosa* LdcA (Q9HTZ1), *N. gonorrhoeae* (YP_208343.1), and *C. jejuni* Pgp2 (WP_002856863) were performed using Clustal Omega (https://www.ebi.ac.uk/Tools/msa/clustalo/) and MView (https://www.ebi.ac.uk/Tools/msa/mview/). Pairwise sequence alignments were performed and amino acid identities among Ldc homologues were calculated by EMBOSS Needle (https://www.ebi.ac.uk/Tools/psa/emboss_needle/). The Prokaryotic Genome Analysis Tool (PGAT) (http://tools.uwgenomics.org/pgat/), BlastP, and BlastX analyses (http://blast.ncbi.nlm.nih.gov) were used to identify *F. tularensis* homologues. Bacterial protein sub-localization was predicted by PSORTb version 3.0.2 (https://www.psort.org/psortb/). Protein signal sequence prediction was performed by LipoP version 1.0 (http://www.cbs.dtu.dk/services/LipoP/) and SignalP version 4.1 (http://www.cbs.dtu.dk/services/SignalP-4.1/).

Generation of F. tularensis gene deletion mutants

F. tularensis isogenic deletion mutants were generated by homologous recombination as previously described (Wu, 2015). Briefly, 500 bp regions upstream and downstream from the gene of interest (*FTL1678* or *FTT0101*) were PCR-amplified from *F. tularensis* genomic DNA using the following primers: FTL1678_A and FTL1678_B; FTL1678_C and FTL1678_D; FTT0101_A and FTT0101_B; FTT0101_C and FTT0101_D (Table S7). A FLP recombination target (FRT)-

622 flanked Pfn-kanamycin resistance cassette, FRT-Pfn-kan-FRT, was PCR amplified from pLG66a
623 (Gallagher, 2008) and splicing overlap extension PCR (SOE PCR) was used to join the upstream
624 (A-B) and downstream (C-D) regions with FRT-Pfn-kan-FRT, which replaced the gene of interest.
625 The resulting insert and a suicide plasmid, pTP163 (Robertson, 2013), were digested with ApaI
626 (New England Biolabs), and ligated using T4 DNA ligase (New England Biolabs). Gene deletion
627 constructs were transformed into NEB10-β *E. coli* (New England Biolabs), sequence-verified,
628 transformed into *E. coli* S17-1, and conjugation was performed with *F. tularensis* LVS on sMHA
629 plates. Conjugants were recovered on chocolate agar supplemented with 200 mg L^{-1} hygromycin
630 and 100 mg L^{-1} polymyxin B. Individual mutants were selected by sequential plating on sMHA
631 supplemented with 10 mg L^{-1} kanamycin (sMHA-kan10), sMHA-kan10 with 8% (wt/vol) sucrose,
632 and final replica plating onto sMHA containing either 200 mg L^{-1} hygromycin (sMHA-hyg200) or
633 sMHA-kan10. Hyg-sensitive and kan-resistant colonies were sequence verified (referred to
634 hereafter as either Δ*FTL1678* or Δ*FTT0101*).
635
636 *FTL1678 complementation in trans*
637 Complementation *in trans* was performed as previously described, with some modifications (Wu,
638 2016). *FTL1678* was PCR-amplified from *F. tularensis* LVS using primers
639 5'FTL1678_NEBuilder and 3'FTL1678_NEBuilder (Table S7), pQE-60 (Qiagen) was double-
640 digested with NcoI and BglII (New England Biolabs), and the NEBuilder HiFi DNA Assembly
641 Cloning kit was used to ligate the *FTL1678* amplicon and digested pQE-60. The construct was
642 transformed into NEB 10-β *E. coli* and transformants were selected on LB agar supplemented with
643 100 mg L^{-1} ampicillin (LB-amp). Plasmids were purified from individual clones using the Qiagen
644 QIAprep Spin Miniprep kit (Qiagen), diagnostic PCR was performed to confirm insert presence
645 and correct size, and DNA sequencing was performed to verify insert integrity. The resulting

construct, *FTL1678* with a C-terminal 6x histidine tag, was PCR-amplified using primers 5'FTL1678_pFNLTP6 and 3'FTL1678_pFNLTP6 (Table S7), the amplicon and pFNLTP6-gro-GFP (Maier, 2004) were double-digested with XhoI and BamHI (New England Biolabs), and ligated using T4 DNA Ligase. The construct, pFNLTP6-gro-*FTL1678*-6xHis, was transformed into NEB10-β *E. coli*, transformants were selected on LB plates supplemented with 50 mg L^{-1} kanamycin (LB-kan), and DNA sequencing was performed to verify FTL1678-6xHis integrity. Next, the kan resistance gene was removed from Δ*FTL1678* by suspending the strain in 0.5 M sucrose (in 1 mM EDTA, pH 7.5), washing three times, and electroporating the shuttle plasmid pTP405 (Robertson, 2013), which encodes the Flp recombinase to remove FRT-Pfn-kan-FRT from the genome. Bacteria were grown overnight on sMHA-hyg200, hyg-resistant transformants were passaged three times on sMHA, then transformants were replica plated onto sMHA-hyg200 and sMHA-kan10 to confirm sensitivity to both antibiotics (kan-cured Δ*FTL1678*). pFNLTP6-gro-*FTL1678*-6xHis was transformed into kan-cured Δ*FTL1678* by electroporation, transformants were selected on sMHA-kan10, and expression of FTL1678 was confirmed by immunoblot analysis (referred to hereafter as Δ*FTL1678 trans*-complement).

C. jejuni Pgp2 complementation in trans

Complementation of *C. jejuni pgp2* (CJJ81176_0915) into Δ*FTL1678* was performed as described above, with several modifications. The *pgp2* gene, with the FTL1678 signal sequence (amino acid residues 1-29) in place of the native Pgp2 signal sequence (amino acid residues 1-18), was synthesized and inserted in pQE-60 by GenScript USA. pQE-60-*pgp2* was transformed into NEB10-β *E. coli* and selection was performed on LB-amp. Pgp2-6xHis was amplified from pQE-60 using primers 5'FTL1678_pFNLTP6 and 3'FTL1678_pFNLTP6 (Table S7), the amplicon was ligated into similarly digested pFNLTP6, pFNLTP6-gro-*pgp2*-6xHis was transformed into

NEB10-β *E. coli*, and transformants were selected on LB-kan. Plasmids were purified from kan-resistant transformants, sequence verified, then electroporated into kan-cured Δ*FTL1678*. Pgp2 expression was confirmed by immunoblot analysis.

Mouse Infections

All animal studies were approved by the University of Toledo Institutional Animal Care and Use Committee (IACUC). Mouse infections were performed as previously described (Huntley, 2008), with some modifications. Briefly, *F. tularensis* strains were grown on sMHA overnight, transferred to BHI agar for an additional 20-24 h, suspended in sterile PBS, and diluted to the desired concentration (20 to 10^9 CFU/20 µl) based on previous OD_{600} measurements and bacterial enumeration studies. Groups of 4-8 female C3H/HeN mice (6-8 weeks old; Charles River Laboratories) were anesthetized with a ketamine-xylazine sedative and intranasally (i.n.) infected with 20 µl of prepared bacterial suspensions. Bacterial innocula were serially-diluted and plated in quadruplet on sMHA to confirm CFUs. For survival studies, mice were monitored daily, for signs of disease, with health status scores (scale of 1-5, with 1 indicating healthy and 5 indicating mouse found dead) being recorded for each mouse. Moribund mice were humanely euthanized to minimize suffering. To quantitate bacterial tissue burdens, groups of 4 mice were euthanized on days 2 and 5 post-infection, blood was collected by cardiac puncture and plated onto sMHA, lungs, livers, and spleens were aseptically harvested, homogenized, 25 µl of PBS/mg of tissue was added to each tissue, serially-diluted, and dilutions were plated onto sMHA. Following 72 h of incubation, the number of colonies per plate were counted and CFU/mg (tissues) or CFU/ml (blood) were calculated based on tissue weight and dilution factor. For immunization and challenge studies, groups of 4-10 mice were i.n. immunized with either 100-300 CFU LVS or 10^4-10^9 CFU ΔFTL1678, boosted 3-4 weeks later with either 10^3 CFU LVS or 10^9 CFU ΔFTL1678,

694 transported to the ABSL3 facility 3-weeks later, and i.n. challenged with 20-120 CFU of *F.*
695 *tularensis* SchuS4. Mice were monitored daily for signs of disease with health status scores being
696 recorded for each mouse.
697
698 *Membrane Integrity Testing*
699 Sensitivity of LVS, Δ*FTL1678*, FTL1678 *trans*-complement, and the Pgp2 *trans*-complement to
700 various antibiotics, detergents, dyes, and cell wall stressors was determined by disk diffusion
701 assays or in liquid cultures, as previously described (Wu, 2016), with some modifications.
702 Bacterial strains were grown on either sMHA or sMHA-kan10 (ΔFTL1678 and complement
703 strains), scraped and resuspended in sterile PBS, adjusted to an OD_{600} of 0.2 (approx. $9x10^7$
704 CFU/ml), diluted 1:1 in PBS, and 100 µl was plated onto sMHA plates using cotton tipped
705 applicators (Puritan). Sterile paper disks (Whatman; 0.8 mm thick, 6.5 mm in diameter) were
706 placed in the center of each plate and antibiotics, detergents, or dyes were added to the disks at the
707 concentrations listed in Table 2. Antibiotics tested were: gentamicin (Gibco), tetracycline (Fisher
708 Scientific), chloramphenicol (Acros Organics), ciprofloxacin (Oxoid), ampicillin (Fisher
709 Scientific), vancomycin (Acros Organics), bacitracin (Oxoid), bacitracin (Oxoid), ciprofloxacin
710 (Oxoid), and polymyxin b (MP Biomedicals). Detergents tested were: sodium dodecyl sulfate
711 (SDS; anionic; Fisher Scientific), Triton X-100 (nonionic; Acros Organics), cetyltrimethyl
712 ammonium bromide (CTAB; cationic; MP Biomedicals), 3-cholamidopropyl dimethylammonio
713 1-propanesulfonate (CHAPS; zwitterionic; Thermo Scientific). In addition, sensitivity to ethidium
714 bromide (Thermo Scientific) and lysozyme (Thermo Fisher) also was tested. After 48 h, diameters
715 of zones of inhibition around the disks were measured. Experiments were performed in triplicate.
716 For liquid cultures, bacteria were suspended in sMHB, adjusted to OD_{600} 0.4, and 5 ml of each
717 bacterial suspensions was inoculated into 100 ml of either sMHB or sMHB with 5 mM hydrogen

peroxide (H_2O_2), 5% sodium chloride (NaCl), or pH 5.5 (pH of sMHB is 6.5). Cultures were grown at 37˚C with rotation at 180 rpm for 24 h with OD_{600} readings recorded every 4 hours.

Electron Microscopy

Electron microscopy was used to visualize differences in bacterial envelope structure and cell shape, as previously described (Wu, 2016), with some modifications. LVS, Δ*FTL1678*, FTL1678 *trans*-complement, and the Pgp2 *trans*-complement were grown overnight in sMHB, approx. $1x10^9$ CFU of each bacterial strain was pelleted by centrifugation at 7000 × *g* at 4˚C, washed three times in PBS, fixed in 3% (vol/vol) glutaraldehyde (Electron Microscopy Sciences [EMS]) for approx. 24 hours, washed twice in sodium cacodylate buffer (pH 7.4; EMS) for 10 min, suspended in 1% (wt/vol) osmium tetroxide (EMS) in s-collidine buffer (pH 7.4; EMS) for 45 min at room temperature (r/t) to stain and fix the samples, washed two times with sodium cacodylate buffer for 10 min each, and tertiary fixation was performed using an aqueous saturated solution of uranyl acetate (pH 3.3; EMS) for 45 min at r/t. Samples were then dehydrated at room temperature using a series of ethanol washes: two washes with 30% ethanol for 10 min each; two washes with 50% ethanol for 10 min each; two washes with 95% ethanol for 10 min each; two washes with 100% ethanol for 10 min each; and two washes with 100% acetone for 10 min each. Samples were then infiltrated with 50% acetone and 50% embedding media (Hard Plus Resin 812, EMS) for 8 h to overnight at r/t. Samples were embedded in 100% embedding media (EMS) and allowed to polymerize for 8 h to overnight at 85°C, then sectioned at 85–90 nm, and visualized using a Tecnai G2 Spirit transmission electron microscope (FEI) at 80 kV and Radius 1.3 (Olympus) camera software at the University of Toledo Electron Microscopy Facility. Experiments were performed twice to confirm reproducibility, with two bacterial preparations fixed, stained, embedded, sectioned, and visualized per experiment.

742

743 *Spheroplasting and Sucrose Density Gradient Centrifugation*

744 Spheroplasting, osmotic lysis, and sucrose density gradient centrifugation was performed as
745 previously described (Huntley, 2007) to determine subcellular localization of FTL1678. Briefly,
746 the histidine-tagged FTL1678 *trans*-complement was grown in sMHB to an OD_{600} of 0.3-0.4,
747 pelleted at 7500 × *g* for 30 min at 10˚C, supernatants were removed, pellets were resuspended in
748 0.75 M sucrose (in 5 mM Tris, pH 7.5) with gentle mixing, 10 mM EDTA (in 5 mM Tris, pH 7.8)
749 was slowly added over 10 min, and the suspension was incubated for 30 min at r/t. After
750 incubation, lysozyme was slowly added to a final concentration of 200 µg ml^{-1}, incubated for 30
751 min at r/t, bacteria were osmotically lysed by dilution into 4.5 × volume of molecular-grade water
752 (Corning) over 11 min with gentle mixing, and incubated for 30 min at r/t. Lysates were
753 centrifuged at 7,500 × *g* for 30 min at 10°C to remove intact cells and cellular debris. Supernatants
754 were collected and centrifuged at 182,500 × *g* for 2 h at 4°C in a F37L 8 × 100 Fiberlite
755 Ultracentrifuge rotor. Following centrifugation, supernatants were removed, membrane pellets
756 were gently resuspended in 6 ml of resuspension buffer (25% [wt/wt] sucrose, 5 mM Tris, 30 mM
757 $MgCl_2$, 1 tablet of Pierce Protease Inhibitor Mini Tablets, EDTA-Free [Thermo Scientific], 5 U
758 Benzonase [Novagen]), suspensions were incubated with gentle mixing for 30 min at room
759 temperature to degrade DNA, and a DC protein assay (Bio-Rad) was performed to determine total
760 protein yield. Linear sucrose gradients were prepared by layering 1.8 ml each of sucrose solutions
761 (wt/wt; prepared in 5 mM EDTA, pH 7.5) into 14- by 95-mm ultracentrifuge tubes (Beckman) in
762 the following order: 55%, 50%, 45%, 40%, 35%, and 30%. Membrane suspensions were layered
763 on top of each sucrose gradient, with less than 1.5 mg of protein per gradient. Sucrose gradients
764 were centrifuged in an SW40 swinging bucket rotor (Beckman) at 256,000 × *g* for 17 h at 4°C.
765 After centrifugation, 500 µl fractions were collected from each gradient by puncturing the bottom

766 of each tube and allowing fractions to drip into microcentrifuge tubes. The refractive index of
767 each fraction was determined using a refractometer (Fisher Scientific) and correlated with a
768 specific density in g ml^{-1} (Price, 1982) to identify outer membrane (OM; 1.17-1.20 g/ml) and inner
769 membrane (IM; 1.13-1.14 g/ml) fractions. Sucrose gradient fractions were examined by
770 immunoblotting as described below.
771
772 *Immunoblotting*
773 Whole cell lysates of FTL1678 *trans*-complement were prepared by suspending bacteria (pelleted
774 at 7000 × *g*) in molecular biology grade water, diluting with SDS-PAGE loading buffer, and
775 boiling for 10 min. Whole cell lysates, OM fractions, IM fractions, and molecular mass standards
776 (Precision Plus protein all blue prestained protein standards; BioRad Laboratories) were separated
777 on a 12.5% polyacrylamide gel, transferred to nitrocellulose, and blots were incubated overnight
778 in blot block (0.1% (vol/vol) Tween 20 and 2% (wt/vol) bovine serum albumin in PBS) at 4°C.
779 Immunoblotting was performed using rat polyclonal antiserum specific for either *F. tularensis* OM
780 protein FopA, *F. tularensis* IM protein SecY (Huntley, 2007) or the Penta-His HRP conjugate
781 antibody (Qiagen).
782
783 *Infections of Mouse Bone Marrow Derived Macrophages (mBMDMs) and J774A.1 cells*
784 Macrophage culture (37˚C with 5% CO_2 unless otherwise indicated) and infections were
785 performed as previously described (Wu, 2016), with some modifications. Bone marrow
786 macrophages were harvested from female C3H/HeN mice. Mice were euthanized by CO_2
787 asphyxiation and cervical dislocation. Femurs and tibias of both hind legs were aseptically-
788 harvested, marrow was flushed from each bone with RPMI-1640 (Hyclone) containing 10% heat-
789 inactivated fetal bovine serum ([HI-FBS], Atlanta Biologicals) and 30% supernatants from day 7

790 L929 cultures (ATCC). Bone marrow was disrupted by repeated passage through a 23-gauge
791 needle and cultured for 4 days. Next, cell media was removed and replaced with RPMI containing
792 10% HI-FBS and 30% supernatant from day 14 L929 cultures, and cells were cultured for 2 days.
793 Approx. 24 h before infection, media was removed, cells were harvested by scraping and
794 centrifugation at 400 × *g* for 10 min at 10˚C, cells were enumerated using a hemocytometer, and
795 diluted to $1x10^5$ cells in RPMI containing 10% HI-FBS. J774A.1 cells (ATCC) were cultured in
796 Dulbecco's Modified Eagle Medium ([DMEM], Gibco) containing 10% HI-FBS. Approx. 24 h
797 before infection, cells were harvested as described above, seeded into individual wells of 24-well
798 plates (Corning) at a concentration of $1x10^5$ cells/well, and incubated overnight. mBMDMs and
799 J774A.1 cells were infected with a multiplicity of infection (MOI) of 100 bacteria to 1 cell (100:1).
800 Following infection, cells were centrifuged at 1,000 × *g* for 10 min at 4˚C, incubated at 37˚C with
801 5% CO_2 for 1 h, washed 1 × with RPMI (or DMEM), media containing 100 μg ml^{-1} gentamicin
802 was added to kill extracellular bacteria, cells were incubated at 37˚C with 5% CO_2 for 1 h, washed
803 1x with RPMI (or DMEM), lysed with 1% saponin for 4 min, serially diluted in PBS, plated onto
804 sMHA plates, and bacteria were enumerated (entry) after 48h. Alternatively, after gentamicin
805 treatment and washing, RPMI (or DMEM) containing 10% HI-FBS was added to cells and they
806 were incubated for 6 or 24 h, lysed, serially-diluted, and plated to determine bacterial numbers.
807
808 *Expression and Purification of Recombinant FTL1678 and FTT0101*
809 *F. tularensis* LVS and SchuS4 genomic DNA were extracted using phenol/chloroform/isoamyl
810 alcohol (Fisher Bioreagents). *FTL1678* and *FTT0101*, without signal sequences (amino acid
811 residues 1-29), were PCR-amplified from LVS and SchuS4 genomic DNA, respectively, using
812 High Fidelity Platinum Taq Polymerase (Life Technologies), and primers 5'FTL1678_BamHI and
813 3'FTL1678_XhoI and 5'FTT0101_BamHI and 3'FTT0101_XhoI, respectively (Table S7).

814 Amplicons and pPROEX HTb were double-digested with BamHI and XhoI, ligated using T4 DNA
815 ligase, and transformed into NEB 10-β *E. coli*. Plasmids were purified using the Qiagen QIAprep
816 Spin Miniprep kit and diagnostic PCR was performed to confirm presence and correct size of the
817 insert. DNA sequencing was performed to confirm insert integrity and plasmid constructs were
818 transformed into Rosetta DE3 *E. coli* (Millipore) for protein expression. Recombinant proteins
819 were expressed and purified as previously described (Ren, 2014) with some modifications.
820 Bacteria were grown in LB-amp to an OD_{600} of 0.4, protein expression was induced for 2 h by the
821 addition of isopropyl β-D-thiogalactopyranoside (IPTG) to a final concentration of 100 mM,
822 bacteria were pelleted by centrifugation, and frozen overnight at −80°C to aid in lysis. Cell pellets
823 were suspended in 10 mM Tris, 500 mM NaCl, and 10 mM imidazole, pH 8.0, sonicated on ice
824 for 10 min with 30 sec intervals, insoluble material was removed by centrifugation at 8,000 × *g*,
825 and supernatants were collected for affinity purification over pre-equilibrated Ni-nitrilotriacetic
826 acid (Ni-NTA) agarose (Qiagen) columns. Eluted recombinant proteins were concentrated in
827 Amicon Ultra-4 centrifugal filter units with 30-kDa cutoff (Millipore), concentrations were
828 determined using the DC BCA protein assay (BioRad), and purity was assessed by SDS-PAGE
829 and Imperial protein staining (Thermo Scientific). An empty vector construct also was expressed
830 and purified as a control in enzymatic assays.
831
832 *Enzymatic Assays for FTL1678/FTT0101 Activity*
833 FTL1678 and FTT0101 recombinant protein activity toward various PG-related compounds were
834 tested in 50 µl reaction mixtures containing 50 mM Tris-HCl, pH 8.0, 0.1 mM substrate, and
835 partially purified enzyme stock (10 µl in 1 M NaCl, 10 mM Tris, pH 8.0). Mixtures were incubated
836 for 30 min to 2 h at 37°C and reactions were stopped by freezing. Substrate and reaction products
837 were separated by HPLC on an ODS-Hypersil 3 µm particle-size C18 column (250 by 4.6 mm;

838 Thermo Scientific). Elutions were performed with 50 mM sodium phosphate buffer, pH 4.5, with
839 or without application of a linear gradient of methanol (from 0 to 50% in 50 min), at a flow rate of
840 0.5 ml/min. Peaks were detected by measuring the absorbance at 207 nm or at 262 nm for UDP-
841 containing nucleotide precursors. Identification of compounds was based on their retention times,
842 compared to authentic standards, as well as on their amino acid and amino sugar composition,
843 determined with a Hitachi model L8800 analyzer (Sciencetec) after hydrolysis of samples in 6 M
844 HCl for 16 h at 95°C. Enzyme activity was calculated by integration of peaks corresponding to
845 substrate and product. Amounts of alanine released by the L,D-carboxypeptidase activity also
846 were determined using an amino acid analyzer. Depending on the substrate used, the amount of
847 partially purified protein varied from 0.9 to 5 µg per assay and incubation times varied from 30
848 min to 4 h. To ensure linearity, substrate consumption was < 20% in all cases. Values represent
849 the means for three independent experiments; the standard deviation was < 10% in all cases.
850 Specific activities were calculated from the amounts of D-Ala (tetrapeptide substrates) or D-Ala-
851 D-Ala (pentapeptide substrates) released during the reaction. FTL1678 double and triple active
852 site mutants were tested in 50 µl reaction mixtures containing 50 mM Tris-HCl, pH 8.0, 0.05 mM
853 substrate, and partially purified enzyme stock (5-10 µl in 1 M NaCl, 10 mM Tris, pH 8.0).
854 Reactions were incubated for 18 hours then analyzed by HPLC as described above. Peaks were
855 detected by measuring absorbance at 207 nm.
856
857 *Peptidoglycan Precursors and Muropeptides*
858 UDP-MurNAc-pentapeptide precursors containing either *meso*-diaminopimelic acid (A_2pm) or L-
859 lysine were prepared by enzymatic synthesis using purified Mur ligases, and UDP-MurNAc-
860 tetrapeptides were generated by treatment of the UDP-MurNAc-pentapeptide precursors with
861 purified *E. coli* PBP5 DD-carboxypeptidase as previously described (Herve, 2007). MurNAc-

862 peptides were obtained by mild acid hydrolysis of UDP-MurNAc-peptides (0.1 M HCl, 100°C, 15
863 min) and were not reduced and thus purified as a mixture of the two α and β anomers (Blanot,
864 1983). Free peptides were prepared by cleavage of MurNAc-peptides with *E. coli* AmiD *N*-
865 acetylmuramoyl-L-alanine amidase (Pennartz, 2009). The *E. coli* peptidoglycan polymer was
866 purified from a Δ*lpp* mutant strain that does not express the Lpp lipoprotein (Leulier, 2003).
867 GlcNAc-1,6-anhydro-MurNAc-L-Ala-γ-D-Glu-*meso*-A_2pm-D-Ala (TCT) and its dimer (two
868 cross-linked TCT monomers) were produced by digestion of peptidoglycan with *E. coli* SltY lytic
869 transglycosylase and the non-anhydro forms of these monomer and dimer were generated by
870 digestion of the polymer with mutanolysin (Stenbak, 2004). All these compounds were HPLC-
871 purified and their composition was controlled by amino acid and amino sugar content analysis
872 and/or by MALDI-TOF mass spectrometry.
873
874 *Statistics*
875 GraphPad Prism6 was used in various statistical analyses, including: differences in antibiotic,
876 detergent, dye, or lysozyme susceptibility were calculated by one-way ANOVA with multiple
877 comparisons and the Holm-Sidak post-hoc test; differences in EM measurements were determined
878 by unpaired t-tests; differences in median time-to-death and percent survival following *F.*
879 *tularensis* infection of mice were calculated using the log-rank Mantel-Cox test; differences in
880 pathology scores of *F. tularensis*-infected tissues were calculated by two-way ANOVA with
881 multiple comparisons and a Tukey post-hoc test. Differences in lung, liver, spleen, and blood
882 bacterial burdens from infected mice were calculated by one-way ANOVA with multiple
883 comparisons using R software.
884
885

Acknowledgments

We would like to acknowledge Drs. Joe Dillard and Ryan Schaub (University of Wisconsin-Madison) for all their help and expertise with peptidoglycan isolation/purification. We would also like to thank Dr. Erin Gaynor for her generous contribution of *C. jejuni* Pgp2-pGEM plasmid construct. This work was supported by grant R01 AI093351 from the National Institute of Allergy and Infectious Disease of the National Institutes of Health (NIAID-NIH) to J.F.H.

Data Availability Statement

Data that support the findings of this study are available in the supplementary material of this article.

References

Blanot, D., Kretsovali A, Abo-Ghalia M, Mengin-Lecreulx D, van Heijenoort J (1983) Synthesis of analogues of precursors of bacterial peptidoglycan, in Malon, B. a. P. (ed), *Peptides*. Berlin, Germany: Walter de Gruyter, 311-314.

Bouveret, E., Benedetti H, Rigal A, Loret E, Lazdunski C (1999) In vitro characterization of peptidoglycan-associated lipoprotein (PAL)-peptidoglycan and PAL-TolB interactions. *J Bacteriol*, 181(20), 6306-11.

Braun, V. (1975) Covalent lipoprotein from the outer membrane of *Escherichia coli*. *Biochim Biophys Acta*, 415(3), 335-77.

Braun, V. & Hantke, K. (2019) Lipoproteins: Structure, Function, Biosynthesis. *Subcell Biochem*, 92, 39-77.

910 Braun, V., Rehn K (1969) Chemical characterization, spatial distribution and function of a
911 lipoprotein (murein-lipoprotein) of the *E. coli* cell wall. The specific effect of trypsin on
912 the membrane structure. *Eur J Biochem*, 10(3), 426-38.
913 Braun, V. & Rehn, K. (1969) Chemical characterization, spatial distribution and function of a
914 lipoprotein (murein-lipoprotein) of the *E. coli* cell wall. The specific effect of trypsin on
915 the membrane structure. *Eur J Biochem*, 10(3), 426-38.
916 Chaput, C., Ecobichon C, Pouradier N, Rousselle JC, Namane A, Boneca IG (2016) Role of the
917 N-Acetylmuramoyl-l-Alanyl Amidase, AmiA, of *Helicobacter pylori* in Peptidoglycan
918 Metabolism, Daughter Cell Separation, and Virulence. *Microb Drug Resist*, 22(6), 477-
919 86.
920 Clavel, T., Germon P, Vianney A, Portalier R, Lazzaroni JC (1998) TolB protein of *Escherichia*
921 *coli* K-12 interacts with the outer membrane peptidoglycan-associated proteins Pal, Lpp
922 and OmpA. *Mol Microbiol*, 29(1), 359-67.
923 Das, D., Herve M, Elsliger MA, Kadam RU, Grant JC, Chiu HJ, Knuth MW, Klock HE, Miller
924 MD, Godzik A, Lesley SA, Deacon AM, Mengin-Lecreulx D, Wilson IA (2013)
925 Structure and function of a novel LD-carboxypeptidase a involved in peptidoglycan
926 recycling. *J Bacteriol*, 195(24), 5555-66.
927 De Pascalis, R., Hahn A, Brook HM, Ryden P, Donart N, Mittereder L, Frey B, Wu TH, Elkins
928 KL (2018) A panel of correlates predicts vaccine-induced protection of rats against
929 respiratory challenge with virulent *Francisella tularensis*. *PLoS One*, 13(5), e0198140.
930 de Pedro, M., Cava F (2015) Structural constraints and dynamics of bacterial cell wall
931 architecture. *Front Microbiol*, 6, 449.
932 den Blaauwen, T., de Pedro MA, Nguyen-Disteche M, Ayala JA (2008) Morphogenesis of rod-
933 shaped sacculi. *FEMS Microbiol Rev*, 32(2), 321-44.

934 Dennis, D., Inglesby TV, Henderson DA, Bartlett JG, Ascher MS, Eitzen E, Fine AD,
935 Friedlander AM, Hauer J, Layton M, Lillibridge SR, McDade JE, Osterholm MT,
936 O'Toole T, Parker G, Perl TM, Russell PK, and Tonat K (2001) Tularemia as a biological
937 weapon: medical and public health management. *JAMA*, 285(21), 2763-73.
938 Denome, S., Elf PK, Henderson TA, Nelson DE, Young KD (1999) *Escherichia coli* mutants
939 lacking all possible combinations of eight penicillin binding proteins: viability,
940 characteristics, and implications for peptidoglycan synthesis. *J Bacteriol*, 181(13), 3981-
941 93.
942 Dhar, S., Kumari H, Balasubramanian D, Mathee K. (2018) Cell-wall recycling and synthesis in
943 *Escherichia coli* and *Pseudomonas aeruginosa* - their role in the development of
944 resistance. *J Med Microbiol*, 67(1), 1-21.
945 Ellis, J., Oyston PC, Green M, Titball RW (2002) Tularemia. *Clin Microbiol Rev*, 15(4), 631-46.
946 Frirdich, E., Biboy J, Adams C, Lee J, Ellermeier J, Gielda LD, Dirita VJ, Girardin SE, Vollmer
947 W, Gaynor EC (2012) Peptidoglycan-modifying enzyme Pgp1 is required for helical cell
948 shape and pathogenicity traits in *Campylobacter jejuni. PLoS Pathog*, 8(3), e1002602.
949 Frirdich, E., Vermeulen J, Biboy J, Soares F, Taveirne ME, Johnson JG, DiRita VJ, Girardin SE,
950 Vollmer W, Gaynor EC (2014) Peptidoglycan LD-carboxypeptidase Pgp2 influences
951 *Campylobacter jejuni* helical cell shape and pathogenic properties and provides the
952 substrate for the DL-carboxypeptidase Pgp1. *J Biol Chem*, 289(12), 8007-18.
953 Gallagher, L., McKevitt M, Ramage ER, Manoil C (2008) Genetic dissection of the *Francisella*
954 *novicida* restriction barrier. *J Bacteriol*, 190(23), 7830-7.
955 Glauner, B., Holtje JV, Schwarz U (1988) The composition of the murein of *Escherichia coli*. *J*
956 *Biol Chem*, 263(21), 10088-95.

957 Guinane, C., Cotter PD, Ross RP, Hill C (2006) Contribution of penicillin-binding protein
958 homologs to antibiotic resistance, cell morphology, and virulence of *Listeria*
959 *monocytogenes* EGDe. *Antimicrob Agents Chemother*, 50(8), 2824-8.
960 Hall, J., Woolard MD, Gunn BM, Craven RR, Taft-Benz S, Frelinger JA, Kawula TH (2008)
961 Infected-host-cell repertoire and cellular response in the lung following inhalation of
962 *Francisella tularensis* Schu S4, LVS, or U112. *Infect Immun*, 76(12), 5843-52.
963 Heidrich, C., Templin MF, Ursinus A, Merdanovic M, Berger J, Schwarz H, de Pedro MA,
964 Holtje JV (2001) Involvement of N-acetylmuramyl-L-alanine amidases in cell separation
965 and antibiotic-induced autolysis of *Escherichia coli*. *Mol Microbiol*, 41(1), 167-78.
966 Heidrich, C., Ursinus A, Berger J, Schwarz H, Holtje JV (2002) Effects of multiple deletions of
967 murein hydrolases on viability, septum cleavage, and sensitivity to large toxic molecules
968 in *Escherichia coli*. *J Bacteriol*, 184(22), 6093-9.
969 Herve, M., Boniface A, Gobec S, Blanot D, Mengin-Lecreulx D (2007) Biochemical
970 characterization and physiological properties of *Escherichia coli* UDP-N-
971 acetylmuramate:L-alanyl-gamma-D-glutamyl-meso-diaminopimelate ligase. *J Bacteriol*,
972 189(11), 3987-95.
973 Holtje, J. (1998) Growth of the stress-bearing and shape-maintaining murein sacculus of
974 *Escherichia coli. Microbiol Mol Biol Rev*, 62(1), 181-203.
975 Huntley, J., Conley PG, Hagman KE, Norgard MV (2007) Characterization of *Francisella*
976 *tularensis* outer membrane proteins. *J Bacteriol*, 189(2), 561-74.
977 Huntley, J., Conley PG, Rasko DA, Hagman KE, Apicella MA, Norgard MV (2008) Native
978 outer membrane proteins protect mice against pulmonary challenge with virulent type A
979 *Francisella tularensis. Infect Immun*, 76(8), 3664-71.

980 Jenkins, C., Wallis R, Allcock N, Barnes KB, Richards MI, Auty JM, Galyov EE, Harding SV,
981 Mukamolova GV (2019) The lytic transglycosylase, LtgG, controls cell morphology and
982 virulence in *Burkholderia pseudomallei. Sci Rep*, 9(1), 11060.
983 Johnson, J., Fisher JF, Mobashery S (2013) Bacterial cell-wall recycling. *Ann N Y Acad Sci*,
984 1277, 54-75.
985 Jones, A. S., Austerberry, J. I., Dajani, R., Warwicker, J., Curtis, R., Derrick, J. P. & Robinson,
986 C. (2016) Proofreading of substrate structure by the Twin-Arginine Translocase is highly
987 dependent on substrate conformational flexibility but surprisingly tolerant of surface
988 charge and hydrophobicity changes. *Biochim Biophys Acta*, 1863(12), 3116-3124.
989 Jones, C., Napier BA, Sampson TR, Llewellyn AC, Schroeder MR, Weiss DS (2012) Subversion
990 of host recognition and defense systems by *Francisella* spp. *Microbiol Mol Biol Rev*,
991 76(2), 383-404.
992 Juan, C., Torrens G, Barcelo IM, Oliver A (2018) Interplay between Peptidoglycan Biology and
993 Virulence in Gram-Negative Pathogens. *Microbiol Mol Biol Rev*, 82(4), e00033-18.
994 Keim, P., Johansson A, Wagner DM (2007) Molecular epidemiology, evolution, and ecology of
995 *Francisella*. *Ann N Y Acad Sci*, 1105, 30-66.
996 Kijek, T., Mou S, Bachert BA, Kuehl KA, Williams JA, Daye SP, Worsham PL, Bozue JA
997 (2019) The D-alanyl-d-alanine carboxypeptidase enzyme is essential for virulence in the
998 Schu S4 strain of *Francisella tularensis* and a dacD mutant is able to provide protection
999 against a pneumonic challenge. *Microb Pathog*, 137, 103742.
1000 Kingry, L., Petersen JM (2014) Comparative review of *Francisella tularensis* and *Francisella*
1001 *novicida*. *Front Cell Infect Microbiol*, 4, 35.

1002 Knodler, L. A., Vallance, B. A., Hensel, M., Jackel, D., Finlay, B. B. & Steele-Mortimer, O.
1003 (2003) *Salmonella* type III effectors PipB and PipB2 are targeted to detergent-resistant
1004 microdomains on internal host cell membranes. *Mol Microbiol*, 49(3), 685-704.
1005 Korza, H., Bochtler M (2005) *Pseudomonas aeruginosa* LD-carboxypeptidase, a serine peptidase
1006 with a Ser-His-Glu triad and a nucleophilic elbow. *J Biol Chem*, 280(49), 40802-12.
1007 Leduc, M., Ishidate K, Shakibai N, Rothfield L (1992) Interactions of *Escherichia coli*
1008 membrane lipoproteins with the murein sacculus. *J Bacteriol*, 174(24), 7982-8.
1009 Lenz, J., Hackett KT, Dillard JP (2017) A Single Dual-Function Enzyme Controls the Production
1010 of Inflammatory NOD Agonist Peptidoglycan Fragments by *Neisseria gonorrhoeae*.
1011 *MBio*, 8(5), e01464-17.
1012 Lenz, J. D., Hackett, K. T. & Dillard, J. P. (2017) A Single Dual-Function Enzyme Controls the
1013 Production of Inflammatory NOD Agonist Peptidoglycan Fragments by *Neisseria*
1014 *gonorrhoeae*. *MBio*, 8(5).
1015 Leulier, F., Parquet C, Pili-Floury S, Ryu JH, Caroff M, Lee WJ, Mengin-Lecreulx D, Lemaitre
1016 B (2003) The *Drosophila* immune system detects bacteria through specific peptidoglycan
1017 recognition. *Nat Immunol*, 4(5), 478-84.
1018 Lund, P., Tramonti, A. & De Biase, D. (2014) Coping with low pH: molecular strategies in
1019 neutralophilic bacteria. *FEMS Microbiol Rev*, 38(6), 1091-125.
1020 Maier, T., Havig A, Casey M, Nano FE, Frank DW, Zahrt TC (2004) Construction and
1021 characterization of a highly efficient *Francisella* shuttle plasmid. *Appl Environ*
1022 *Microbiol*, 70(12), 7511-9.
1023 Mengin-Lecreulx, D. & Lemaitre, B. (2005) Structure and metabolism of peptidoglycan and
1024 molecular requirements allowing its detection by the *Drosophila* innate immune system.
1025 *J Endotoxin Res*, 11(2), 105-11.

Metz, R., Henning S, Hammes WP (1986a) LD-carboxypeptidase activity in *Escherichia coli*. I. The LD-carboxypeptidase activity in ether treated cells. *Arch Microbiol*, 144(2), 175-80.

Metz, R., Henning S, Hammes WP (1986b) LD-carboxypeptidase activity in *Escherichia coli*. II. Isolation, purification and characterization of the enzyme from *E. coli* K 12. *Arch Microbiol*, 144(2), 181-6.

Meyer, K., Addy C, Akashi S, Roper DI, Tame JRH (2018) The crystal structure and oligomeric form of *Escherichia coli* L,D-carboxypeptidase A. *Biochem Biophys Res Commun*, 499(3), 594-599.

Minor, P. (2015) Live attenuated vaccines: Historical successes and current challenges. *Virology*, 479-480, 379-92.

Mishra, S. & Imlay, J. (2012) Why do bacteria use so many enzymes to scavenge hydrogen peroxide? *Arch Biochem Biophys*, 525(2), 145-60.

Nelson, D., Young KD (2000) Penicillin binding protein 5 affects cell diameter, contour, and morphology of *Escherichia coli*. *J Bacteriol*, 182(6), 1714-21.

Park, J., Uehara T (2008) How bacteria consume their own exoskeletons (turnover and recycling of cell wall peptidoglycan). *Microbiol Mol Biol Rev*, 72(2), 211-27.

Pazos, M. & Peters, K. (2019) Peptidoglycan. *Subcell Biochem*, 92, 127-168.

Pennartz, A., Genereux C, Parquet C, Mengin-Lecreulx D, Joris B (2009) Substrate-induced inactivation of the *Escherichia coli* AmiD N-acetylmuramoyl-L-alanine amidase highlights a new strategy to inhibit this class of enzyme. *Antimicrob Agents Chemother*, 53(7), 2991-7.

Petrosino, J. F., Xiang, Q., Karpathy, S. E., Jiang, H., Yerrapragada, S., Liu, Y., Gioia, J., Hemphill, L., Gonzalez, A., Raghavan, T. M., Uzman, A., Fox, G. E., Highlander, S., Reichard, M., Morton, R. J., Clinkenbeard, K. D. & Weinstock, G. M. (2006)

1050 Chromosome rearrangement and diversification of *Francisella tularensis* revealed by the
1051 type B (OSU18) genome sequence. *J Bacteriol*, 188(19), 6977-85.
1052 Price, C. (1982) Centrifugation in density gradients. *Academic Press*, 335-343.
1053 Priyadarshini, R., de Pedro MA, Young KD (2007) Role of peptidoglycan amidases in the
1054 development and morphology of the division septum in *Escherichia coli*. *J Bacteriol*,
1055 189(14), 5334-47.
1056 Priyadarshini, R., Popham DL, Young KD (2006) Daughter cell separation by penicillin-binding
1057 proteins and peptidoglycan amidases in *Escherichia coli*. *J Bacteriol*, 188(15), 5345-55.
1058 Qin, A., Scott DW, Thompson JA, Mann BJ (2009) Identification of an essential *Francisella*
1059 *tularensis* subsp. *tularensis* virulence factor. *Infect Immun*, 77(1), 152-61.
1060 Ray, K., Marteyn B, Sansonetti PJ, Tang CM (2009) Life on the inside: the intracellular lifestyle
1061 of cytosolic bacteria. *Nat Rev Microbiol*, 7(5), 333-40.
1062 Ren, G., Champion MM, Huntley JF (2014) Identification of disulfide bond isomerase substrates
1063 reveals bacterial virulence factors. *Mol Microbiol*, 94(4), 926-44.
1064 Roberts, L., Powell DA, Frelinger JA (2018) Adaptive Immunity to *Francisella tularensis* and
1065 Considerations for Vaccine Development. *Front Cell Infect Microbiol*, 8, 115.
1066 Robertson, G., Child R, Ingle C, Celli J, Norgard MV (2013) IglE is an outer membrane-
1067 associated lipoprotein essential for intracellular survival and murine virulence of type A
1068 *Francisella tularensis*. *Infect Immun*, 81(11), 4026-40.
1069 Russo, T., MacDonald U, Beanan JM, Olson R, MacDonald IJ, Sauberan SL, Luke NR, Schultz
1070 LW, Umland TC (2009) Penicillin-binding protein 7/8 contributes to the survival of
1071 *Acinetobacter baumannii* in vitro and in vivo. *J Infect Dis*, 199(4), 513-21.
1072 Scheurwater, E., Reid CW, Clarke AJ (2008) Lytic transglycosylases: bacterial space-making
1073 autolysins. *Int J Biochem Cell Biol*, 40(4), 586-91.

1074 Silhavy, T. J., Kahne, D. & Walker, S. (2010) The bacterial cell envelope. *Cold Spring Harb*
1075 *Perspect Biol*, 2(5), a000414.
1076 Sjostedt, A. (2007) Tularemia: history, epidemiology, pathogen physiology, and clinical
1077 manifestations. *Ann N Y Acad Sci*, 1105, 1-29.
1078 Spidlova, P., Stojkova P, Dankova V, Senitkova I, Santic M, Pinkas D, Philimonenko V, Stulik J
1079 (2018) *Francisella tularensis* D-Ala D-Ala Carboxypeptidase DacD Is Involved in
1080 Intracellular Replication and It Is Necessary for Bacterial Cell Wall Integrity. *Front Cell*
1081 *Infect Microbiol*, 8, 111.
1082 Steiner, D., Furuya Y, Jordan MB, Metzger DW (2017) Protective Role for Macrophages in
1083 Respiratory *Francisella tularensis* Infection. *Infect Immun*, 85(6).
1084 Stenbak, C., Ryu JH, Leulier F, Pili-Floury S, Parquet C, Herve M, Chaput C, Boneca IG, Lee
1085 WJ, Lemaitre B, Mengin-Lecreulx D (2004) Peptidoglycan molecular requirements
1086 allowing detection by the *Drosophila* immune deficiency pathway. *J Immunol*, 173(12),
1087 7339-48.
1088 Sycuro, L., Pincus Z, Gutierrez KD, Biboy J, Stern CA, Vollmer W, Salama NR (2010)
1089 Peptidoglycan crosslinking relaxation promotes *Helicobacter pylori*'s helical shape and
1090 stomach colonization. *Cell*, 141(5), 822-33.
1091 Sycuro, L., Rule CS, Petersen TW, Wyckoff TJ, Sessler T, Nagarkar DB, Khalid F, Pincus Z,
1092 Biboy J, Vollmer W, Salama NR (2013) Flow cytometry-based enrichment for cell shape
1093 mutants identifies multiple genes that influence *Helicobacter pylori* morphology. *Mol*
1094 *Microbiol*, 90(4), 869-83.
1095 Templin, M., Ursinus A, Holtje JV (1999) A defect in cell wall recycling triggers autolysis
1096 during the stationary growth phase of *Escherichia coli*. *EMBO J*, 18(15), 4108-17.

1097 Typas, A., Banzhaf M, Gross CA, Vollmer W (2011) From the regulation of peptidoglycan
1098 synthesis to bacterial growth and morphology. *Nat Rev Microbiol*, 10(2), 123-36.
1099 Ursinus, A., Steinhaus H, Holtje JV (1992) Purification of a nocardicin A-sensitive LD-
1100 carboxypeptidase from *Escherichia coli* by affinity chromatography. *J Bacteriol*, 174(2),
1101 441-6.
1102 van Heijenoort, J. (2011) Peptidoglycan hydrolases of *Escherichia coli*. *Microbiol Mol Biol Rev*,
1103 75(4), 636-63.
1104 Vollmer, W. & Bertsche, U. (2008) Murein (peptidoglycan) structure, architecture and
1105 biosynthesis in *Escherichia coli*. *Biochim Biophys Acta*, 1778(9), 1714-34.
1106 Walburger, A., Lazdunski C, Corda Y (2002) The Tol/Pal system function requires an interaction
1107 between the C-terminal domain of TolA and the N-terminal domain of TolB. *Mol*
1108 *Microbiol*, 44(3), 695-708.
1109 Wu, X., Ren G, Gunning WT 3rd, Weaver DA, Kalinoski AL, Khuder SA, Huntley JF (2016)
1110 FmvB: A *Francisella tularensis* Magnesium-Responsive Outer Membrane Protein that
1111 Plays a Role in Virulence. *PLoS One*, 11(8), e0160977.
1112 Wu, X., Ren G, Huntley JF (2015) Generating Isogenic Deletions (Knockouts) in *Francisella*
1113 *tularensis*, a Highly-infectious and Fastidious Gram-negative Bacterium. *Bio Protoc*,
1114 5(12), e1500.

1115

Table 1. Specific Activity and Substrate Specificity of FTL1678 and FTT0101 Enzymes

Substrate	Specific Activity (nmol/min/mg of protein) [a]	
	FTL1678	FTT0101
A_2pm-containing substrates		
GlcNAc-anhydroMurNAc-L-Ala-γ-D-Glu-*meso*-A_2pm-D-Ala (TCT)	21.5	29.0
GlcNAc-MurNAc-L-Ala-γ-D-Glu-*meso*- A_2pm-D-Ala (PG monomer)	15.6	24.2
TCT dimer	7.7	11.8
MurNAc-L-Ala-γ-D-Glu-*meso*-A2pm-D-Ala	5.8	7.8
UDP-MurNAc-L-Ala-γ-D-Glu-*meso*-A_2pm-D-Ala	4.6	6.3
L-Ala-γ-D-Glu-*meso*-A_2pm-D-Ala (free tetrapeptide)	3.4	8.0
MurNAc-L-Ala-γ-D-Glu-*meso*-A_2pm-D-Ala-D-Ala (pentapeptide)	9.8	6.2
UDP-MurNAc-L-Ala-γ-D-Glu-*meso*-A_2pm-D-Ala-D-Ala (pentapeptide)	5.9	6.4
L-Lysine-containing substrates		
MurNAc-L-Ala-γ-D-Glu-L-Lys-D-Ala	1.3	2.1
L-Ala-γ-D-Glu-L-Lys-D-Ala	0.7	2.1
UDP-MurNAc-L-Ala-γ-D-Glu-L-Lys-D-Ala-D-Ala	1.2	1.7
Other		
GlcNAc-MurNAc-L-Ala-γ-D-Glu-*meso*-A_2pm(NH_2)-D-Ala		Very low (<0.5)
GlcNAc-MurNAc-L-Ala-γ-D-Glu(NH_2)-*meso*-A_2pm-D-Ala		Not detected [b]
GlcNAc-MurNAc-L-Ala-γ-D-Glu(NH_2)-*meso*-A_2pm(NH_2)-D-Ala		Not detected [b]
Peptidoglycan polymer		Not detected [b]

[a] Standard enzyme assay conditions are described in the Materials and Methods.

[b] Not detected indicates that no release of alanine was detected.

Table 2. Sensitivity of WT and Δ*FTL1678* to Antibiotics, Detergents, and Dyes

Compound	Concentration (µg/disk)	Average Zone of Inhibition, mm (mean ± SD)[a]		
		WT	**Δ*FTL1678***	
Gentamicin	4	2.50 ± 0.10	0.93 ± 0.15	(R)
Tetracycline	5	1.83 ± 0.06	0.80 ± 0.00	(R)
Chloramphenicol	5	3.37 ± 0.12	1.00 ± 0.00	(R)
Ciprofloxacin	5	4.73 ± 0.23	1.90 ± 0.10	(R)
Ampicillin	200	2.57 ± 0.12	3.53 ± 0.15	(S)
Vancomycin	20	1.27 ± 0.21	2.60 ± 0.10	(S)
Bacitracin	182	1.10 ± 0.10	1.20 ± 0.10	
Polymyxin B	100	0.70 ± 0.00	0.70 ± 0.00	
Lysozyme	1000	0.70 ± 0.00	1.67 ± 0.06	(S)
Ethidium Bromide	5	2.73 ± 0.15	0.80 ± 0.00	(R)
Triton-X100	750	3.40 ± 0.27	2.63 ± 0.06	(R)
SDS	1000	1.20 ± 0.10	1.80 ± 0.00	(S)
CTAB	50	0.73 ± 0.06	0.80 ± 0.10	
CHAPS	50	0.70 ± 0.00	0.70 ± 0.00	

[a] (R) indicates Δ*FTL1678* is significantly more resistant than WT by one-way ANOVA ($P<0.05$)

[a] (S) indicates Δ*FTL1678* is significantly more sensitive than WT by one-way ANOVA ($P<0.05$)

Figure 1. Amino acid alignment of bacterial L,D-carboxypeptidases. Clustal Omega amino acid alignment of *E. coli* LdcA (BAA36050.1), *P. aeruginosa* LdcA (Q9HTZ1), *N. gonorrhoeae* LdcA (YP_208343.1), *F. tularensis* Type B FTL1678, and *F. tularensis* Type A FTT0101, and *C. jejuni* Pgp2 (WP_002856863). Percent identities (pid), compared to *E. coli* LdcA, are indicated. Black shading indicates similar residues. Red shading indicates the catalytic triad.

Figure 2. FTL1678 is OM-associated. Spheroplasting, osmotic lysis, and sucrose density gradient centrifugation were performed to separate inner membranes (IM) and outer membranes (OM) from *F. tularensis* ΔFTL1678 *trans*-complemented with a 6× histidine-tagged FTL1678. Whole-cell lysates (WCL), OM fractions, and IM fractions were separated by SDS-PAGE, transferred to nitrocellulose, and immunoblotting was performed using antisera specific for the OM control protein FopA (αFopA), IM control protein SecY (αSecY), or histidine-tagged FTL1678.

Figure 3. FTL1678 controls bacterial morphology. Electron micrograph images of: (A) Wild-type LVS or (B) Δ*FTL1678* grown in sMHB to OD_{600} of 0.4. Scale bars represent 100 nm; (C) Outer membrane thickness measurements (nm) were measured for WT and Δ*FTL1678*, n=50; (D) Cell width measurements (nm) for WT and Δ*FTL1678*, n=175. **** indicates $P<0.0001$.

Figure 4. Deletion of *FTL1678* increases resistance to stressors. WT and Δ*FTL1678* were grown in 75 ml sMHB at: (A) 37˚C, (B) sMHB at 40˚C, (C) sMHB + 60 µM $CuCl_2$, (D) sMHB + 5 mM H_2O_2, (E) sMHB + 5% NaCl, or (F) sMHB at pH 5.5. Bacteria were grown for 24 hours and OD_{600} measurements were recorded every 4 hours.

Figure 5. ΔFTL1678 is fully-attenuated in a mouse pulmonary infection model. (A) Groups of 5 C3H/HeN mice were intranasally-infected with 10^5 CFU of either wild-type WT, Δ*FTL1678*, or Δ*FTL1678* *trans*-complemented with *FTL1678* [FTL1678 compl]. Animal health was monitored daily through day 21 post-infection. **** indicates $P<0.0001$; (B) Lungs, livers, spleens, and blood were aseptically harvested from mice infected with 10^4 CFU of either WT or Δ*FTL1678* on days 2 and 5 post-infection and plated to enumerate bacterial numbers. * indicates $P<0.01$; (C) Groups of 5 C3H/HeN mice were intranasally-infected with 10^5 CFU of either LVS, Δ*FTL1678*, FTL1678 *trans*-complement [FTL1678 compl], or *C. jejuni* Pgp2 *trans*-complement [Pgp2 compl]. Animal health was monitored through day 21 post-infection. ** indicates $P<0.01$.

Figure 6. FTL1678 is required for *F. tularensis* replication in macrophages. (A) J774A.1 macrophages or mouse bone marrow-derived macrophages (mBMDMs) were infected with WT or Δ*FTL1678* at an MOI of 100:1 and bacterial numbers were enumerated at entry (0 h), 6 h, and 24 h post-infection. (B) Fold change in bacterial numbers from 6 to 24 h post-infection was calculated. * indicates $P< 0.01$.

Figure 7. Δ*FTL1678* protects against fully-virulent Type A *F. tularensis* SchuS4. (A) Groups of 5 C3H/HeN mice were intranasally infected with either 10^5 CFU WT or 10^5, 10^7, or 10^9 CFU Δ*FTL1678*. On day 29 post-infection, mice were boosted with 10^9 CFU Δ*FTL1678* and animal health was monitored daily through day 50 post-infection. *** $P<0.001$; (B) Mice from A were intranasally-challenged with 120 CFU of wild-type SchuS4 [BSL3; 6× LD50]. Animal health was monitored daily through day 26 post-infection. * indicates $P<0.001$.

Figure 8. Δ*FTL1678* does not induce tissue damage. (A) Hematoxylin and eosin (H&E)-stained lungs, livers, and spleens were examined from either uninfected, *F. tularensis* WT LVS-, or Δ*FTL1678*-infected mice at 10× objective. (B) Tissues were graded on a scale of 0 to 4, with 4 being the most severe. * indicates $P<0.05$.

Figure 9. Model of *F. tularensis* peptidoglycan synthesis and recycling pathways. Bioinformatic analyses were used to predict proteins that may be involved in peptidoglycan synthesis and recycling in *F. tularensis*. *F. tularensis* LVS gene locus tags are indicated, with *E. coli* or Gram-negative ortholog protein names. OM, outer membrane. IM, inner membrane. GlcNAc, N-Acetylglucosamine. MurNAc, N-Acetylmuramic acid. Pal, OM-localized peptidoglycan-associated lipoprotein. TolB, periplasmic protein that interacts with Pal and peptidoglycan. HMM PBP, high molecular weight penicillin binding protein. LMM PBP, low molecular weight penicillin binding protein.

Supporting Information

Table S1. Bioinformatic analyses of FTL1678 localization

Table S2. Endopeptidase activity of FTL1678

Table S3. Sensitivity of WT *F. tularensis* SchuS4 and Δ*FTT0101* to antibiotics, detergents, and dyes

Table S4. Specific activity of FTL1678, FTL1678 double mutants, and FTL1678 triple mutants to the TCT monomer

Table S5. Sensitivity of WT LVS, ΔFTL1678, FTL1678 trans-complement, and Pgp2 trans-complement to antibiotics, detergents, and dyes

Table S6. Bacterial strains and plasmids used in this study

Table S7. Primers used in this study

Figure S1. FTL1678 contains a putative L,D-carboxypeptidase domain. NCBI Conserved Domain search results for *F. tularensis* FTL1678.

Figure S2. F. tularensis TolB is OM-localized. Spheroplasting, osmotic lysis, and sucrose density gradient centrifugation were performed to separate inner membranes (IM) and outer

membranes (OM) from *F. tularensis* Δ*FTL1678 trans*-complemented with a 6x histidine-tagged FTL1678. Whole-cell lysates (WCL), OM fractions, and IM fractions were separated by SDS-PAGE, transferred to nitrocellulose, and immunoblotting was performed using antisera specific for the periplasmic protein TolB (αTolB).

Figure S3. ΔFTL1678 does not have a growth defect. WT and ΔFTL1678 were grown in sMHB for 24 hours at 37˚C. Samples were taken every 4 hours for (A) OD600 measurements and (B) CFU enumeration following serial-dilution and plating.

Figure S4. ΔFTL1678 has septation defects. Transmission electron micrograph images of ΔFTL1678 showing aberrant septal formation and reduced ability to separate cells. Images taken at: (A) 49,000×, scale bar represents 200 nm; and (B) 6,800×, scale bar represents 2 μm. In (A), red arrows point to formed septa that have not separated in ΔFTL1678 and white arrows point to new septa that are forming in ΔFTL1678. Experiments were performed twice to confirm reproducibility, with two bacterial preparations fixed, stained, embedded, sectioned, and visualized per experiment. Representative images shown.

Figure S5. FTT0101 is not required for *F. tularensis* Type A strain SchuS4 virulence. C3H/HeN mice were intranasally infected with either 80 CFU SchuS4 (n=3 mice) or 12 CFU Δ*FTT0101* (n=5 mice).

Figure S6. LdcA catalytic triad is not essential for *F. tularensis* virulence. Groups of 5 C3H/HeN mice were intranasally-infected with 10^5 CFU of either *F. tularensis* WT LVS, Δ*FTL1678*, Δ*FTL1678 trans*-complemented with FTL1678 (FTL1678 compl), Δ*FTL1678 trans*-

complemented with S134A (S134A), Δ*FTL1678 trans*-complemented with E239A (E239A), or Δ*FTL1678 trans*-complemented with H308A (H308A). Animal health was monitored daily through day 21 post-infection. ** $P<0.01$.

Figure S7. FTL1678 *trans*-complement and *C. jejuni* Pgp2 *trans*-complement restore *F. tularensis* phenotype. Transmission electron micrograph images of: (A) Δ*FTL1678 trans*-complemented with *FTL1678* [FTL1678 compl] or (B) Δ*FTL1678 trans*-complemented with *C. jejuni pgp2* [Pgp2 compl]. Bacteria were grown in sMHB to OD_{600} of 0.4. Scale bars represent 100 nm. (C) Outer membrane thickness and (D) cell width of FTL1678 compl and Pgp2 compl were compared to WT LVS and D*FTL1678.* **** indicates $P<0.0001$.

Figure S8. FTL1678 *trans*-complement and *C. jejuni* Pgp2 *trans*-complement exhibit similar phenotypes to stressors as WT *F. tularensis*. WT LVS [WT], Δ*FTL1678,* Δ*FTL1678 trans*-complemented with *FTL1678* [FTL1678 compl], or Δ*FTL1678 trans*-complemented with *C. jejuni pgp2* [Pgp2 compl] were grown in either: (A) sMHB; (B) sMHB with 5 mM H_2O_2; (C) sMHB with 5% NaCl; or (D) sMHB at pH 5.5. Cultures were incubated for 24 hours and OD_{600} measurements were recorded every 4 hours.

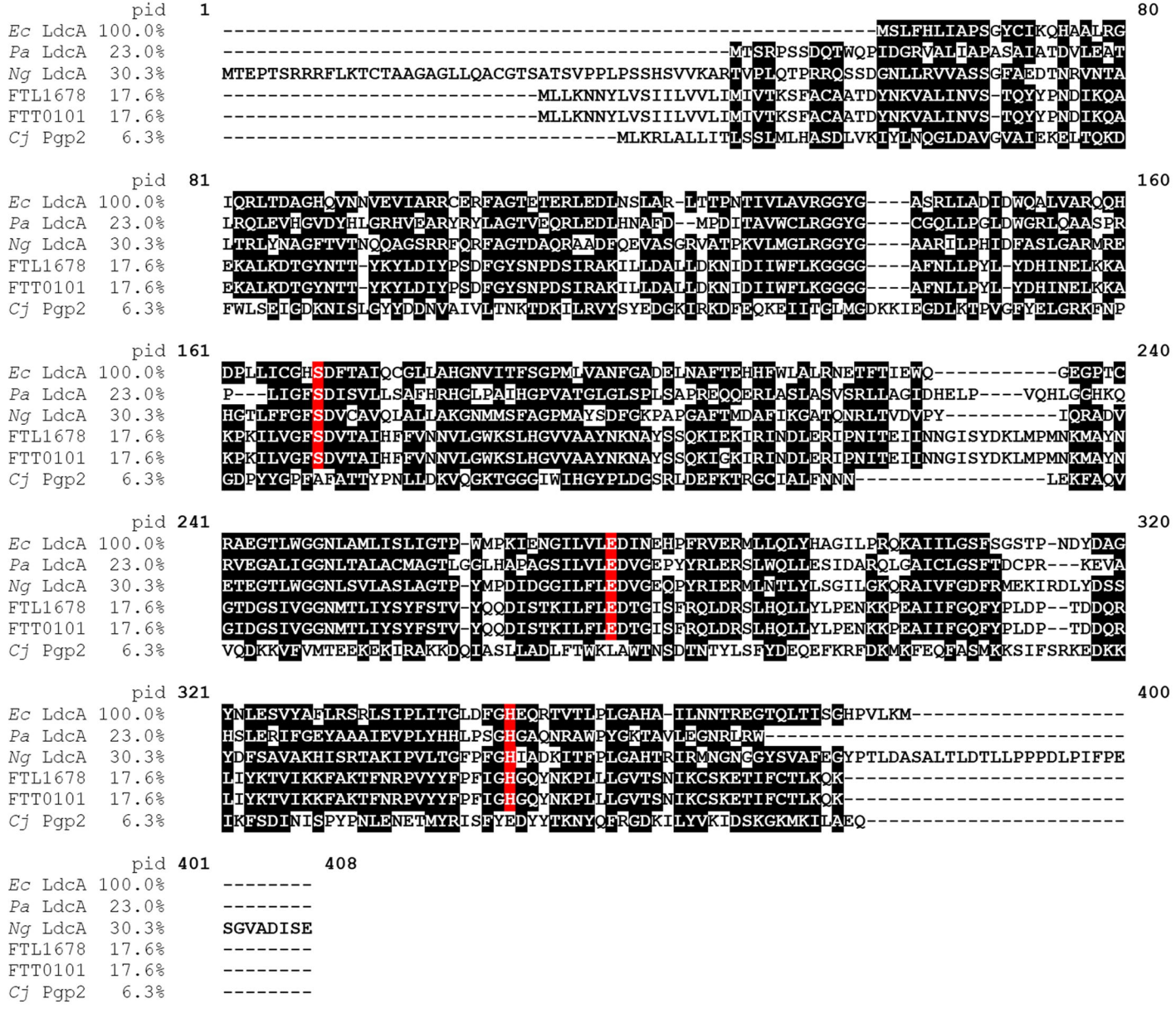
pid 1 80
Ec LdcA 100.0%
Pa LdcA 23.0%
Ng LdcA 30.3%
FTL1678 17.6%
FTT0101 17.6%
Cj Pgp2 6.3%
pid 81 160
pid 161 240
pid 241 320
pid 321 400
pid 401 408
SGVADISE

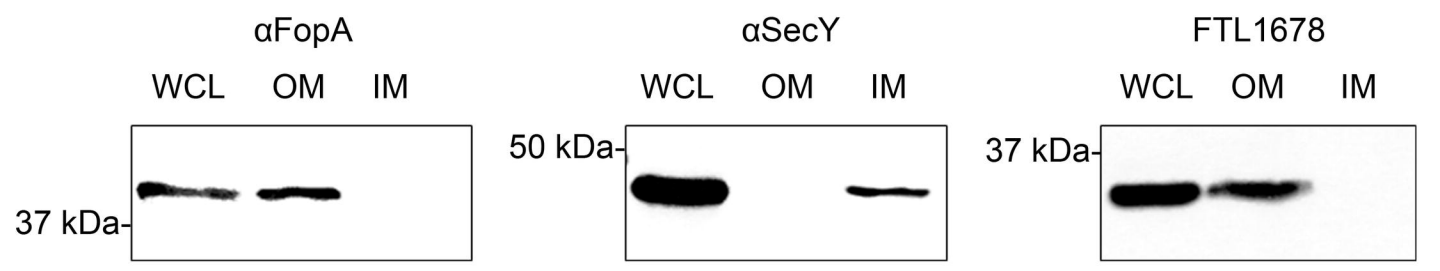
αFopA
WCL
OM
IM
37 kDa
αSecY
WCL
OM
IM
50 kDa
FTL1678
WCL
OM
IM
37 kDa

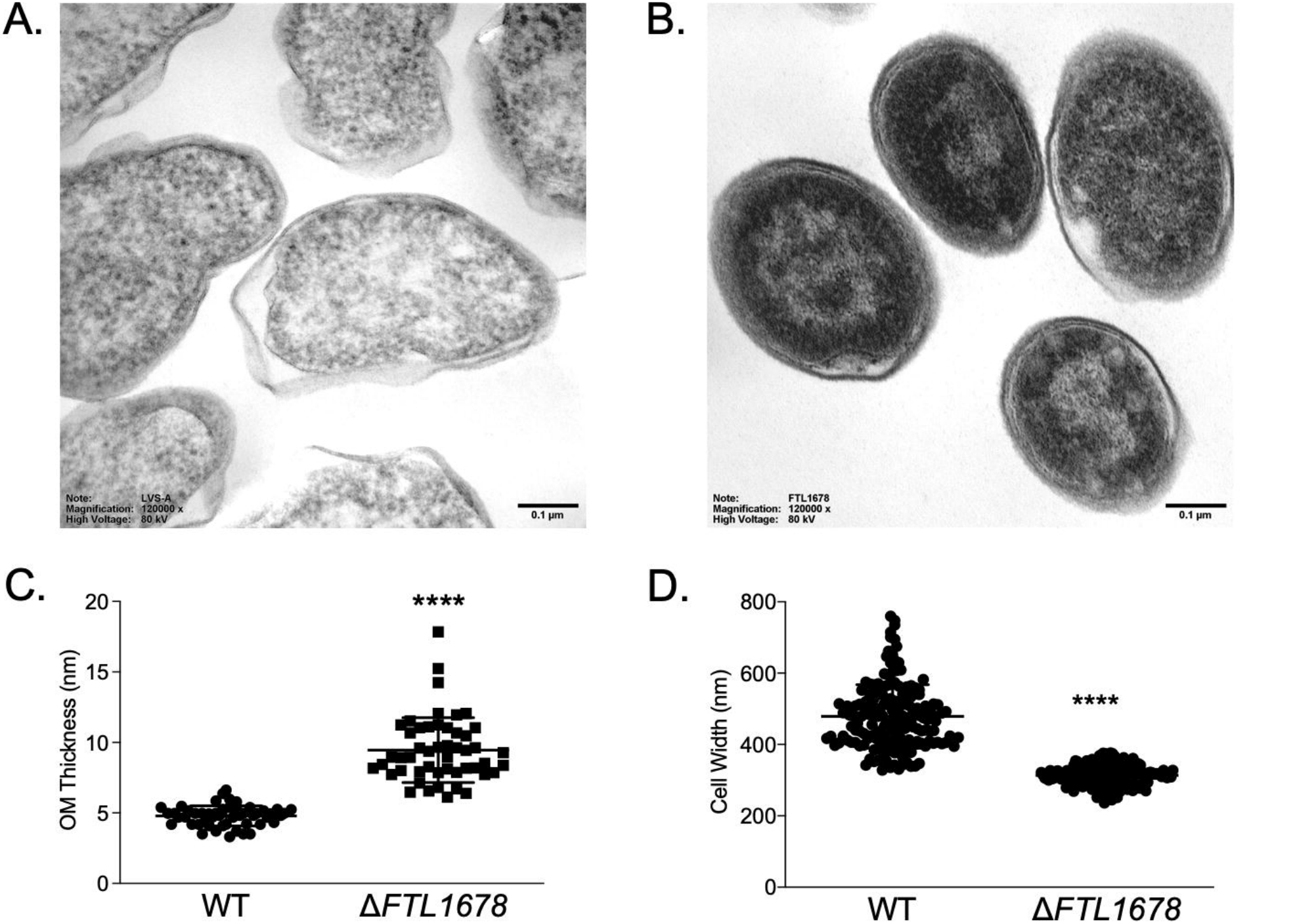
A.
Note: LVS-A
Magnification: 120000 x
High Voltage: 80 kV
0.1 µm
B.
Note: FTL1678
Magnification: 120000 x
High Voltage: 80 kV
0.1 µm
C.
OM Thickness (nm)
20
15
10
5
0
****
WT
ΔFTL1678
D.
Cell Width (nm)
800
600
400
200
0
****
WT
ΔFTL1678

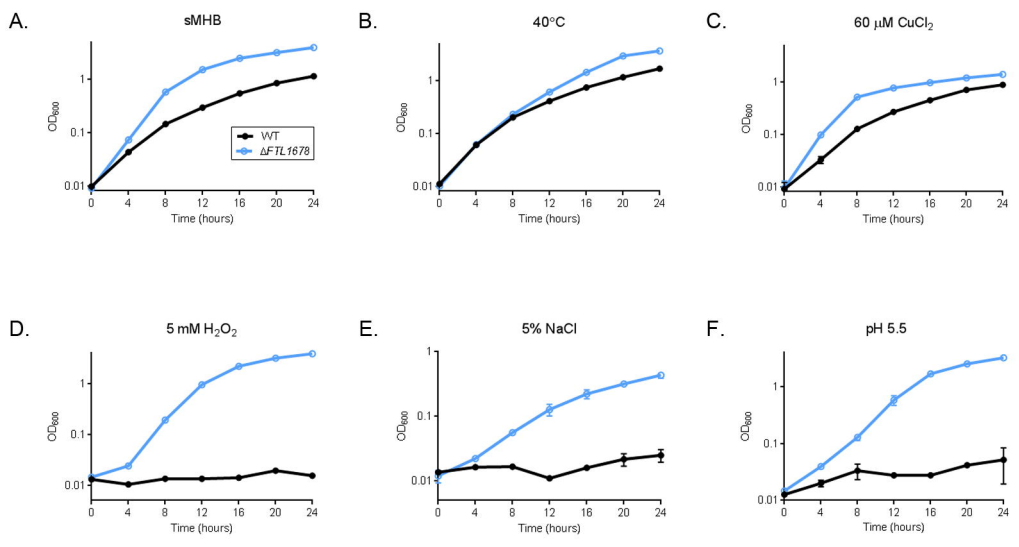
A.
sMHB
B.
40°C
C.
60 μM CuCl2
D.
5 mM H2O2
E.
5% NaCl
F.
pH 5.5
OD600
Time (hours)
WT
ΔFTL1678

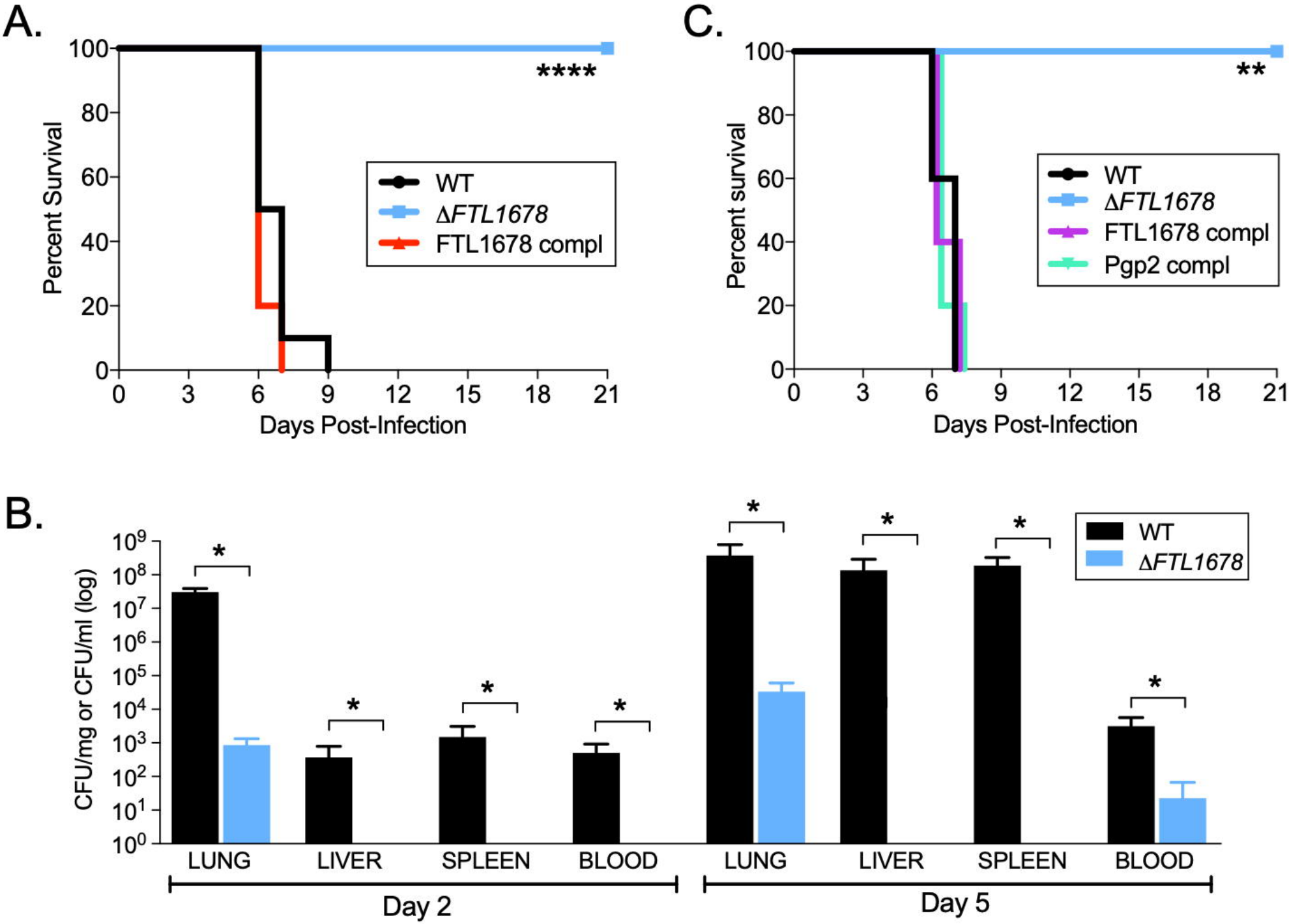
A.
Percent Survival
Days Post-Infection
WT
ΔFTL1678
FTL1678 compl
****
C.
Percent survival
Days Post-Infection
WT
ΔFTL1678
FTL1678 compl
Pgp2 compl
**
B.
CFU/mg or CFU/ml (log)
LUNG
LIVER
SPLEEN
BLOOD
Day 2
Day 5
WT
ΔFTL1678

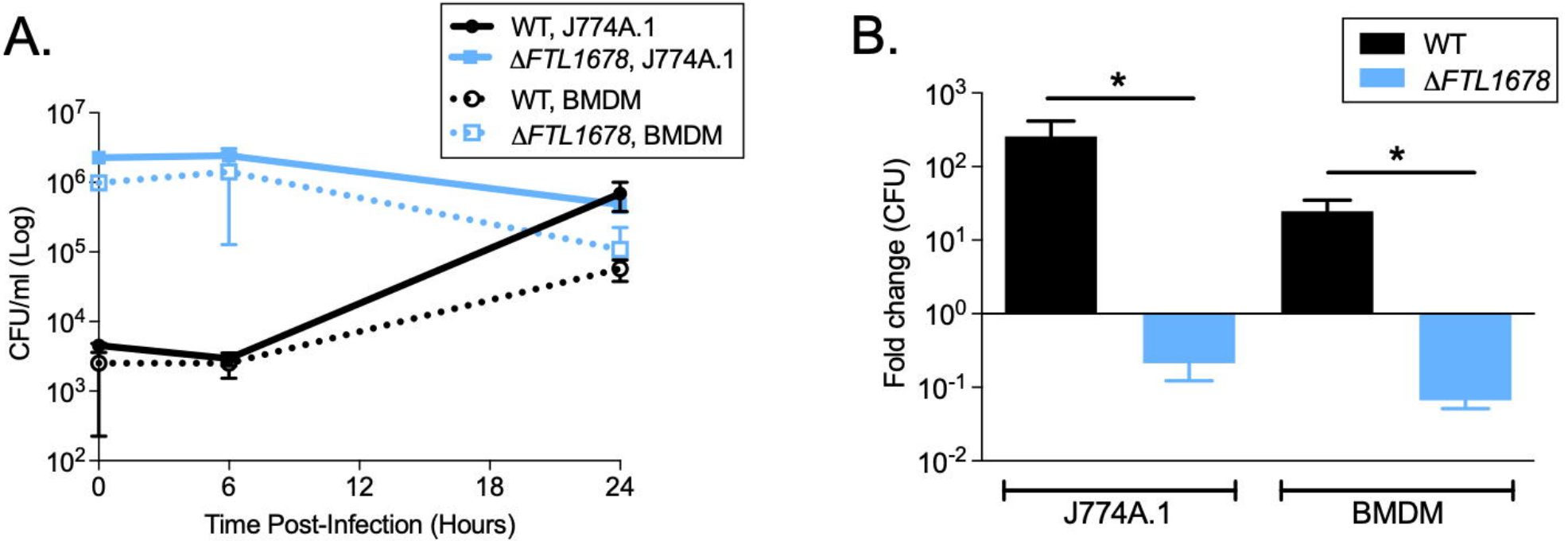
A.
WT, J774A.1
ΔFTL1678, J774A.1
WT, BMDM
ΔFTL1678, BMDM
CFU/ml (Log)
Time Post-Infection (Hours)
B.
WT
ΔFTL1678
Fold change (CFU)
J774A.1
BMDM

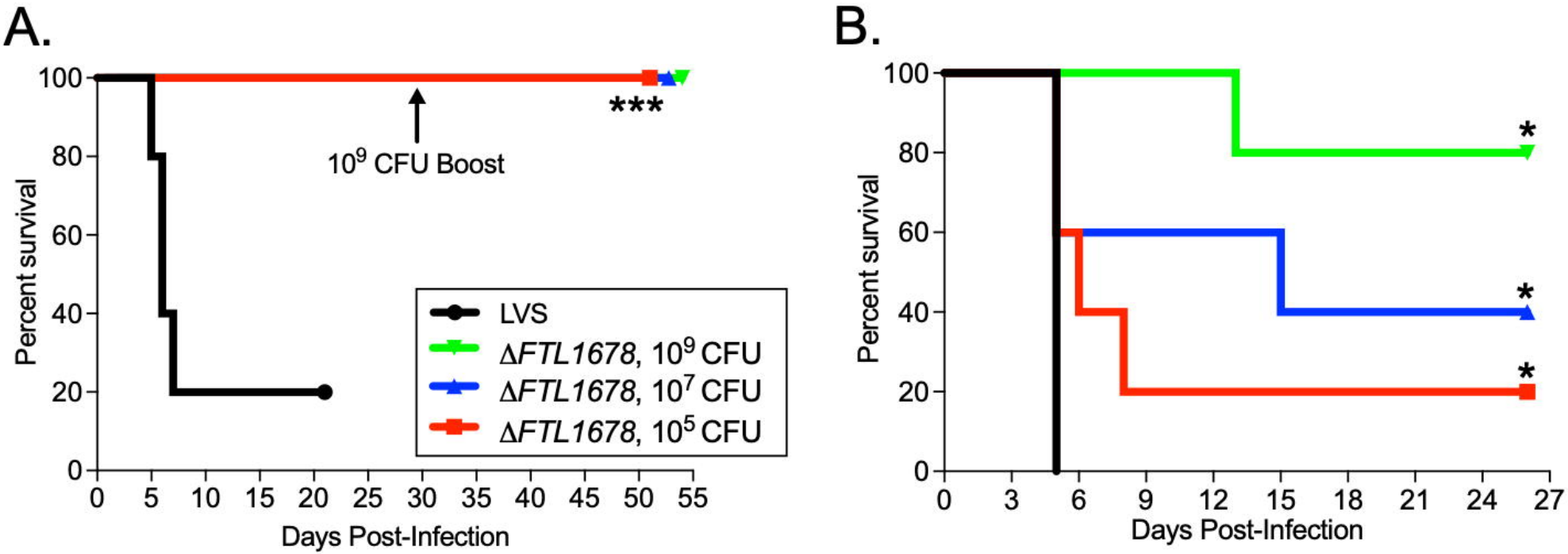
A.
100
80
60
40
20
0
Percent survival
***
10^9 CFU Boost
LVS
ΔFTL1678, 10^9 CFU
ΔFTL1678, 10^7 CFU
ΔFTL1678, 10^5 CFU
0 5 10 15 20 25 30 35 40 45 50 55
Days Post-Infection
B.
100
80
60
40
20
0
Percent survival
*
*
*
0 3 6 9 12 15 18 21 24 27
Days Post-Infection

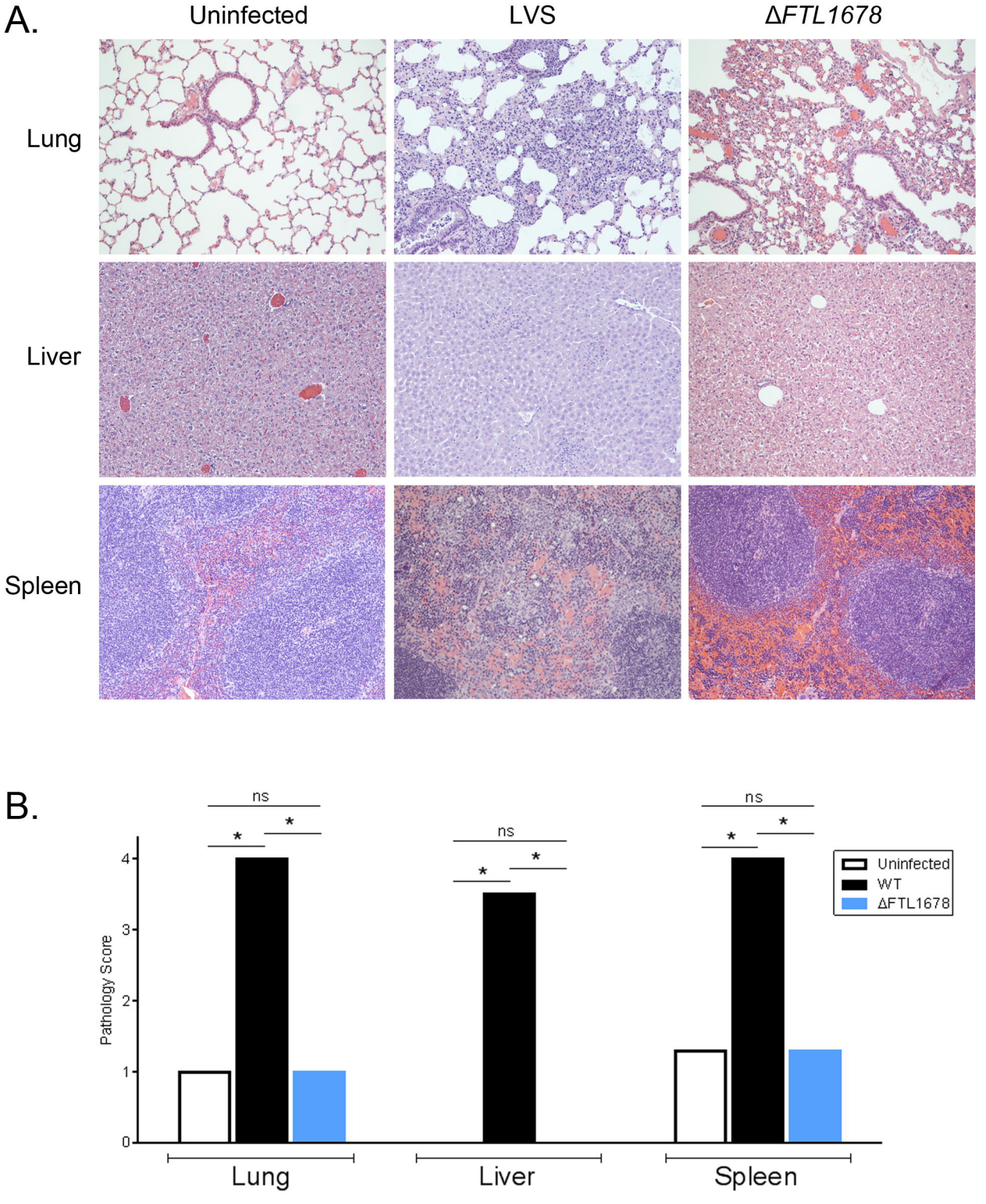
A.
Uninfected
LVS
ΔFTL1678
Lung
Liver
Spleen
B.
ns
*
*
ns
*
*
ns
*
*
Pathology Score
0
1
2
3
4
Uninfected
WT
ΔFTL1678
Lung
Liver
Spleen

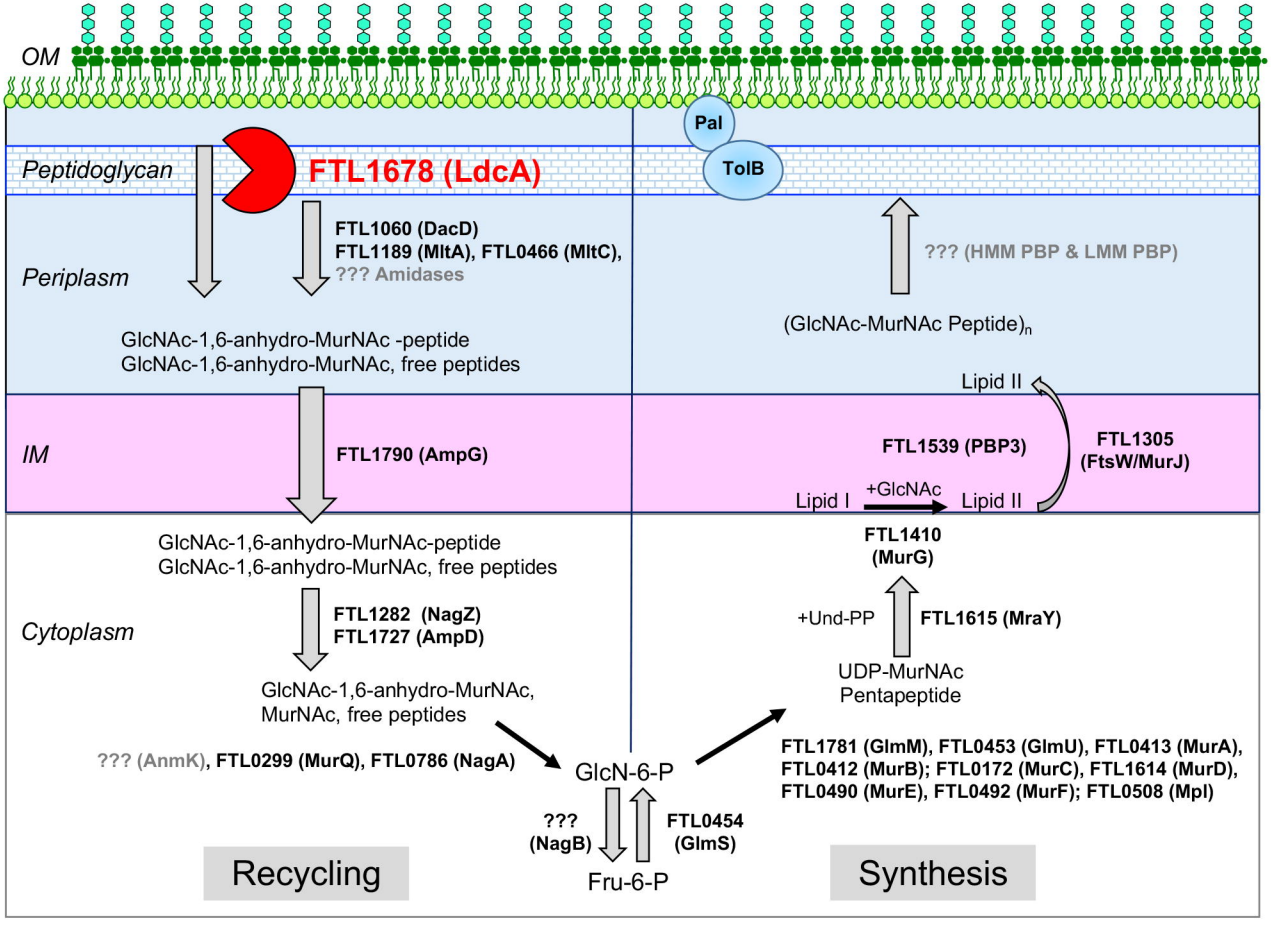
OM
Peptidoglycan
FTL1678 (LdcA)
Pal
TolB
Periplasm
FTL1060 (DacD)
FTL1189 (MltA), FTL0466 (MltC),
??? Amidases
??? (HMM PBP & LMM PBP)
(GlcNAc-MurNAc Peptide)n
GlcNAc-1,6-anhydro-MurNAc -peptide
GlcNAc-1,6-anhydro-MurNAc, free peptides
Lipid II
IM
FTL1790 (AmpG)
FTL1539 (PBP3)
FTL1305
(FtsW/MurJ)
Lipid I
+GlcNAc
Lipid II
FTL1410
(MurG)
GlcNAc-1,6-anhydro-MurNAc-peptide
GlcNAc-1,6-anhydro-MurNAc, free peptides
Cytoplasm
FTL1282 (NagZ)
FTL1727 (AmpD)
+Und-PP
FTL1615 (MraY)
UDP-MurNAc
Pentapeptide
GlcNAc-1,6-anhydro-MurNAc,
MurNAc, free peptides
??? (AnmK), FTL0299 (MurQ), FTL0786 (NagA)
GlcN-6-P
FTL1781 (GlmM), FTL0453 (GlmU), FTL0413 (MurA),
FTL0412 (MurB); FTL0172 (MurC), FTL1614 (MurD),
FTL0490 (MurE), FTL0492 (MurF); FTL0508 (Mpl)
???
(NagB)
FTL0454
(GlmS)
Fru-6-P
Recycling
Synthesis